AIP | Physics of Fluids

A kinetic theory for particulate systems with bimodal and anisotropic velocity fluctuations

Shailesh S. Ozarkar, Ashok S. Sangani, Volodymyr I. Kushch, and Donald L. Koch

Citation: Phys. Fluids **20**, 123303 (2008); doi: 10.1063/1.3035943
View online: http://dx.doi.org/10.1063/1.3035943
View Table of Contents: http://pof.aip.org/resource/1/PHFLE6/v20/i12
Published by the American Institute of Physics.

A kinetic theory for particulate systems with bimodal and anisotropic velocity fluctuations

Shailesh S. Ozarkar,[1] Ashok S. Sangani,[1] Volodymyr I. Kushch,[2] and Donald L. Koch[3]
[1]*Department of Biomedical and Chemical Engineering, Syracuse University, Syracuse, New York 13244, USA*
[2]*Institute of Superhard Materials, National Academy of Sciences of Ukraine, Kiev 254074, Ukraine*
[3]*School of Chemical and Biomolecular Engineering, Cornell University, Ithaca, New York 14853, USA*

(Received 2 July 2008; accepted 27 October 2008; published online 4 December 2008)

Observations of bubbles rising near a wall under conditions of large Reynolds and small Weber numbers have indicated that the velocity component of the bubbles parallel to the wall is significantly reduced upon collision with a wall. To understand the effect of such bubble-wall collisions on the flow of bubbly liquids bounded by walls, a model is developed and examined in detail by numerical simulations and theory. The model is a system of bubbles in which the velocity of the bubbles parallel to the wall is significantly reduced upon collision with the channel wall while the bubbles in the bulk are acted upon by gravity and linear drag forces. The inertial forces are accounted for by modeling the bubbles as rigid particles with mass equal to the virtual mass of the bubbles. The standard kinetic theory for granular materials modified to account for the viscous and gravity forces and supplemented with boundary conditions derived assuming an isotropic Maxwellian velocity distribution is inadequate for describing the behavior of the bubble-phase continuum near the walls since the velocity distribution of the bubbles near the walls is significantly bimodal and anisotropic. A kinetic theory that accounts for such a velocity distribution is described. The bimodal nature is captured by treating the system as consisting of two species with the bubbles (modeled as particles) whose most recent collision was with a channel wall treated as one species and those whose last collision was with another bubble as the other species. The theory is shown to be in very good agreement with the results of numerical simulations and provides closure relations that may be used in the analysis of bidisperse particulate systems as well as bounded bubbly flows. © *2008 American Institute of Physics*. [DOI: 10.1063/1.3035943]

I. INTRODUCTION

Determination of the equations of motion and average properties of bubbly liquids has been a subject of numerous investigations in the past.[1–14] In particular, the special case of flows in which the hydrodynamic interactions among bubbles can be determined using the potential flow approximation has been extensively studied.[8–10,13,15] The potential flow approximation is expected to be valid when the Reynolds number based on the bubble radius and characteristic velocity is large compared with unity but the Weber number, the ratio of inertial to surface tension forces, is small enough so that the bubbles are approximately spherical, and the liquid is free of surface-active impurity.[16–20] This somewhat ideal case can be studied experimentally,[21,22] numerically using large scale simulations which account for the hydrodynamic interactions among bubbles,[15] and analytically using the methods of statistical mechanics[23] and kinetic theory of dense granular materials.[24–33] A complete set of equations of motion derived using these numerical simulations and analytical techniques for spherical bubbles is given by Spelt and Sangani.[10]

These equations of motion must be supplemented with suitable boundary conditions for the bubble-phase continuum in contact with a wall. The numerical simulations cited above were carried out using the usual periodic boundary conditions appropriate for macroscopically homogeneous bubbly liquids. To obtain conditions that must be used when rigid walls are present, one must ideally carry out large scale simulations in wall-confined geometries and extract the macroscopic boundary conditions by comparing the profiles of time-averaged volume fraction, velocity, etc., computed from direct numerical simulations with those obtained using averaged equations of motion. Such numerical simulations and comparison with the averaged equations have been carried out by Nott and Brady[34] for the case of wall-bounded small Reynolds number particulate flows, by Verberg and Koch[35] for high Stokes number and small to moderate Reynolds number suspension flows, and by Galvin *et al.*[36] for the case of rapid granular flows of particles. The potential flow approximation used in numerical simulations of bubbly liquids, however, is not justified in general when rigid walls are present (see, e.g., Ref. 37). We therefore study here a simple model that incorporates some of the important features of the bubble-wall interactions as observed by Tsao and Koch[38] and study in detail the effect of such interactions on the properties of bubbly liquids in the vicinity of a wall including the boundary conditions for the bubble-phase continuum. Although we were initially motivated by its application to bubbly liquids, the problem studied here and the techniques developed here may also be useful in the study of flows of bidisperse granular materials as explained later.

The model we consider is a simple system in which we

ignore the hydrodynamic interactions and treat bubbles as equivalent to solid particles whose mass equals the virtual mass of the bubbles. The component of the velocity of a bubble, henceforth referred to as a particle, parallel to the wall decreases by a constant fraction, $1-\alpha$, upon colliding with the wall. The particle-wall collision also reduces the kinetic energy of the particle by a fixed fraction, $1-\gamma$. The particles in the bulk are acted upon by gravity and linear drag forces, and the particle-particle collisions are perfectly elastic. The neglect of hydrodynamic interactions is a reasonable approximation when the relative velocity of interacting bubbles is large compared with their common velocity. For example, Kang *et al.*[9] found that for sheared bubble suspensions without buoyancy, hard-sphere simulations were in close agreement with simulations of hydrodynamically interacting bubbles. Likewise, Kumaran and Koch[13] found that buoyant bubbles with different terminal velocities would encounter and separate in a manner qualitatively similar to a hard-sphere bounce (although the bubbles did not make actual contact) when the difference of velocities was larger than about 10% of the mean velocity. The wall-bounded bubbly flow considered here will have large velocity differences if, as is generally observed in experiments, α is substantially smaller than 1.

We study in detail the effect of such particle-wall encounters on the velocity fluctuations, volume fraction, and other properties of the system by molecular-dynamics-like simulations. The particle velocity distribution near the walls for such collisions is, in general, significantly bimodal and anisotropic so that the equations of motion and the boundary conditions derived based on the assumption of nearly isotropic Maxwellian velocity distribution do not predict well the behavior of such a system.

We develop a kinetic theory that accounts for both the bimodal and the anisotropic nature of the velocity distribution by treating the particulate system as consisting of two species: particles whose last collision was with other particles and particles whose last collision was with one of the container walls. These are referred to as, respectively, the normal and wall-excited particles. A collision between a wall-excited particle and any other particle converts the wall-excited particle into a normal particle.

Although our initial interest in developing the kinetic theory was to obtain an accurate description appropriate for our model of bubble-wall collisions and its effect on the bubble-phase continuum boundary conditions, we found that our model also provides a stable bidisperse (two-species) system which may serve as a benchmark for testing constitutive relations for bidisperse granular materials.[26,28,33] This is important since the uniform state of most bidisperse systems is unstable and therefore not accessible through direct numerical simulations. The present system allows detailed term-by-term comparison of the predictions of a kinetic theory for two-species materials and the results of numerical simulations. The constitutive relations for bidisperse materials proposed in the literature are shown to lead to significant errors and a number of new ones are proposed. Although the masses and the radii of the colliding particles are taken to be equal in the main body of the text for the sake of simplicity, the expressions for the more general case of inelastic collisions and unequal mass or radius can be readily derived and are summarized in Appendix B.

The model is described in more detail in Sec. II together with representative results of dynamic simulations. A kinetic theory that takes into account the bimodal anisotropic velocity fluctuations is described in Sec. III. Section IV gives detailed term-by-term comparison between the theory and the results of numerical simulations together with constitutive relations for various average quantities and boundary conditions. Section V describes an approximate theory that incorporates closure relations derived in Sec. IV and simplified boundary conditions and compares its predictions with the results of particle dynamics simulations. Finally, Sec. VI summarizes the important findings of the study.

II. NUMERICAL SIMULATIONS AND COMPARISON WITH A STANDARD KINETIC THEORY

Numerical simulations were carried out for a model particulate suspension confined between two rigid, vertical walls at $x_2=\pm h/2$. Periodicity boundary conditions were used along the x_1 and x_3 axes. The bubbles were modeled as rigid, spherical particles of equal size with their mass equivalent to the virtual mass of the bubbles. The collisions between the particles were assumed to be perfectly elastic. Furthermore, since our primary interest was in examining the effect of particle-wall collisions, the hydrodynamic interactions among the particles and the lift force were neglected. Viscous and gravity forces acting on each particle were taken to be the same as for an isolated bubble in an infinite medium. Observations of bubble-wall interactions indicate that the velocity component of the bubbles parallel to the wall significantly reduces upon collision.[38] This was incorporated in our simulations by requiring that the components of the velocity of the particle in the x_1 and x_3 directions be reduced by a factor of α upon collision with the wall, while the component of velocity in the x_2 direction reverses with a magnitude such that the overall kinetic energy after the collision is γ times the energy before the collision with the wall. Thus, the particle velocity satisfies the following collision rule:

$$c_1^+ = \alpha c_1^-, \quad c_3^+ = \alpha c_3^-, \quad c_i^+ c_i^+ = \gamma c_i^- c_i^-, \tag{1}$$

where c_i is the particle velocity. Superscripts $-$ and $+$ refer, respectively, to the velocities before and after a collision with a wall.

The particle motion satisfies

$$m\frac{dc_i}{dt} = m_b \hat{g}_i - \lambda c_i, \tag{2}$$

where $\hat{g}_i$ is the gravitational acceleration (which must be distinguished from the relative velocity g_i used in the kinetic theory described in Sec. III), m is the mass of the particle, $m_b\hat{g}_i$ is the force due to gravity, and λc_i is the viscous force. For the case of a spherical bubble at large Reynolds numbers, $m=-m_b/2=(2\pi/3)a^3\rho_f$ and $\lambda=12\pi\mu_f a$ (Levich drag coefficient), ρ_f and μ_f being, respectively, the density and viscosity of the suspending liquid and a the radius of the bubble. We also introduce the apparent density ρ of the par-

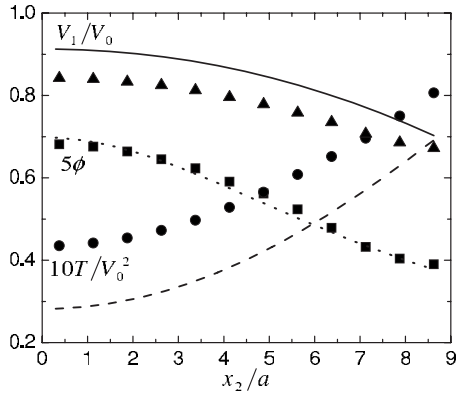

FIG. 1. The profiles of volume fraction, nondimensional velocity, and particle phase temperature for $\langle\phi\rangle=0.1$, $\alpha=0.5$, $\gamma=1$, St=50, and $N=191$. Filled symbols and lines represent, respectively, numerical simulations and simple kinetic theory.

ticle phase as given by $\rho=3m/(4\pi a^3)$. Thus, for the case of bubbles, $\rho=\rho_f/2$ is the density based on its virtual mass. For a particle sedimenting through a gas at low Reynolds numbers, $\rho=\rho_p$, the density of the particle, and $\lambda=6\pi\mu_f a$ (Stokes drag coefficient). Nondimensionalizing the velocity with the terminal velocity $V_0=|m_b|\hat{g}/\lambda$ and the time with a/V_0 results in a nondimensional parameter, the Stokes number, defined by $\mathrm{St}=mV_0/a\lambda$.

Input parameters to the typical numerical simulations were average volume fraction $\langle\phi\rangle$, the wall-collision parameters α and γ, the Stokes number St, and the number of particles, N. Numerical simulations were initiated by placing N particles with randomly chosen, nonoverlapping positions in a unit cell of a vertical channel and their velocities were chosen from an isotropic Maxwellian velocity distribution. Simulations proceeded in time by finding the next pair of colliding particles and their collision time. The positions of the particles were updated based on their current velocities and the minimum of the prescribed time Δt or the time for any two particles or a particle and a wall to collide. The postcollision velocities of the colliding particles were calculated using the model of elastic binary collision of the hard spheres and the collision rule given by Eq. (1) for particle-wall collisions. Simulations were carried out typically for about 50 000 time steps ($\Delta t=0.05a/V_0$) for the particle phase to equilibrate. Next, simulations were carried out for 10^6 additional time steps and various average properties were computed. The presence of the walls induces variations in the average properties along the x_2 direction. The unit cell was divided typically into 24 equal oblong cells parallel to the walls, and various properties of the particle phase were determined by computing averages for each cell.

The results of averaging for a representative case ($\langle\phi\rangle=0.1$, $\alpha=0.5$, $\gamma=1$, St=50, and $N=191$) are shown in Fig. 1. For this case, the ratio of channel width h to particle radius a is about 20. We see that the average nondimensional velocity of the particles over the width of the channel is less than 1, indicating that the presence of the wall causes a reduction in the average velocity of the particles. This is to be expected for $\alpha<1$ for which the particles lose momentum upon collision with one of the channel walls. The resulting shear force imparted by the walls on the particle phase continuum reduces the average velocity. The volume fraction of the particles (recall that the lift force is absent in the present model) is seen to have a maximum at the center of the channel. Figure 1 also shows the variation in the particle phase temperature T defined as

$$T=\mathbf{T}_{ii}/3 \quad \text{with} \quad \mathbf{T}_{ij}=\langle C_iC_j\rangle. \tag{3}$$

Here, $C_i=c_i-V_i$ is the fluctuation velocity of the particle and $V_i=\langle c_i\rangle$ is the average particle velocity at a location. The angular brackets imply time averaging.

The results of numerical simulations will be first compared with a standard kinetic theory with slip boundary conditions. Theories of this type have been shown to yield predictions in good agreement with numerical simulations and experiments for bounded microgravity, granular shear flows of slightly inelastic particles with volume fractions up to 0.5.[39] However, we shall point out significant deficiencies of the standard kinetic theory for wall-bounded buoyancy driven bubbly flows. This will motivate the development of a more detailed kinetic theory in Sec. III.

The conservation equations for the number density, momentum, and fluctuation energy of the particulate phase treated as a continuum are given by[29]

$$\frac{\partial n}{\partial t}+\frac{\partial}{\partial x_j}(nV_j)=0, \tag{4}$$

$$mn\left(\frac{\partial V_i}{\partial t}+V_j\frac{\partial V_i}{\partial x_j}\right)=-\frac{\partial P_{ij}}{\partial x_j}+n(m_b\hat{g}_i-\lambda V_i), \tag{5}$$

$$\frac{3}{2}mn\left(\frac{\partial T}{\partial t}+V_j\frac{\partial T}{\partial x_j}\right)=-\frac{\partial q_j}{\partial x_j}-P_{ij}e_{ij}-3\lambda nT. \tag{6}$$

Here, $n=3\phi/(4\pi a^3)$ is the number density of the particles at a point x_j at time t, V_i the velocity, P_{ij} the particle phase pressure tensor, $e_{ij}=(\partial V_i/\partial x_j+\partial V_j/\partial x_i)/2$, the rate of strain tensor, and q_j the fluctuation energy flux.

The main difficulty arises in providing closure relations for P_{ij} and q_j. The simplest closures correspond to assuming linear relations as given by the kinetic theory of dense gases and used widely in the granular flow literature:[24–33]

$$P_{ij}=mnT(1+4\phi G)\delta_{ij}-[\kappa-(2/3)\mu_s]e_{kk}\delta_{ij}-2\mu_s e_{ij}, \tag{7}$$

$$q_j=-k\frac{\partial T}{\partial x_j}, \tag{8}$$

The shear viscosity μ_s, bulk viscosity κ, and conductivity k are given by

$$\mu_s=\frac{16}{5\pi^{1/2}}mnaT^{1/2}\phi G\left[1+\frac{\pi}{12}\left(1+\frac{5}{8\phi G}\right)^2\right], \tag{9}$$

$$\kappa=\frac{16}{3\pi^{1/2}}mnaT^{1/2}\phi G, \tag{10}$$

$$k = \frac{8}{\pi^{1/2}} mnaT^{1/2}\phi G\left[1 + \frac{9\pi}{32}\left(1 + \frac{5}{12\phi G}\right)^2\right]. \quad (11)$$

In the above equations, δ_{ij} is the Kronecker delta and G is the value of the radial distribution function for particles in contact. The well-known Carnahan–Starling approximation[40] for hard-sphere dense gas molecular system may be used to estimate the radial distribution function at contact:

$$G = \frac{1 - \phi/2}{(1-\phi)^3}. \quad (12)$$

The above equations must be supplemented with boundary conditions for the particle phase continuum. The first condition is that the velocity component normal to the walls must be zero:

$$V_2 = 0 \quad \text{at } x_2 = \pm(h/2 - a). \quad (13)$$

Note that the boundary conditions apply at a distance a from the walls since the centers of the bubbles can at most come within a distance equal to the radius of the bubbles. The boundary condition for the tangential component of the momentum equation is obtained by requiring that the tangential momentum lost due to particle collisions with a wall must be equal to the shear stress at $x_2 = \pm(h/2-a)$. The former can be estimated by assuming that the velocity distribution of the particles near the wall is Maxwellian while the latter can be related to the velocity gradient through Eq. (7). This yields

$$\mp \mu_s \frac{\partial V_1}{\partial x_2} = \frac{(1-\alpha)mnT^{1/2}V_1}{\sqrt{2\pi}} \quad \text{at } x_2 = \pm(h/2 - a). \quad (14)$$

Similarly, the fluctuation energy lost due to particle-wall collisions can be equated to q_2, and hence the temperature gradient, to yield the boundary condition

$$\pm k\frac{\partial T}{\partial x_2} = \frac{mn}{2}\left(\frac{T}{2\pi}\right)^{1/2}[(\gamma - 2\alpha + 1)(V_1)^2 + 4(\gamma - 1)T] \quad \text{at } x_2 = \pm(h/2 - a). \quad (15)$$

Equations (4)–(6) together with the boundary conditions [Eqs. (13)–(15)] were solved using a finite element method. Results of the predictions based on this theory are compared against those obtained by particle dynamics simulations in Fig. 1. We see that while this simple theory captures well the trends for the profiles of particle phase volume fraction, velocity, and temperature, significant quantitative discrepancy exists between the two. We have also carried out simulations for the case when the overall volume fractions are 0.05 and 0.15 and for other values of the Stokes number and found that there is significant quantitative disagreement between the simulation results and the above theory in all the cases examined.

To understand the source of discrepancy, we calculated both the x_1 component of the momentum lost due to collisions and the shear stress ($\tau_{12} = -P_{12}$) by direct numerical simulations. For the case shown in Fig. 1, these two quantities, nondimensionalized by ρV_0^2 ($\rho \equiv mn/\phi$), were both found to equal 0.0043. Thus, simulation results do confirm that the momentum lost due to collisions is equal to the shear stress. In contrast, if we evaluate the momentum lost using the right-hand side (rhs) of Eq. (14) with the values of T, ϕ, and V_1 obtained from numerical simulations (extrapolated to $x_2 = h/2 - a$), we obtain 0.0029, a value that is about 33% lower than the simulation result. Likewise, the nondimensional shear stress, evaluated using the left-hand side (lhs) of Eq. (14) and the simulation results for $\partial V_1/\partial x_2$ and μ_s estimated using the dense gas expression Eq. (9), gave 0.0013, about 70% lower than the stress determined directly from simulations. Thus, we conclude that both the assumption of an isotropic Maxwellian velocity distribution used for estimating the momentum lost due to collision and the assumption of a Newtonian stress tensor with the viscosity determined from the dense gas theory are not justified for the present system.

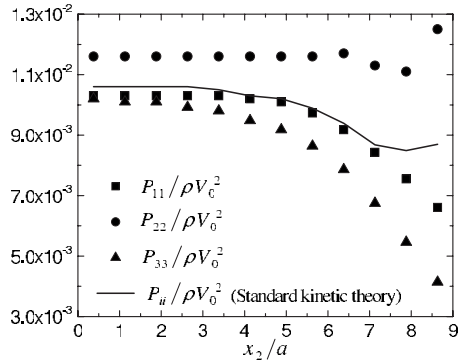

FIG. 2. The variation of individual components of pressure tensor with x_2. Filled symbols represent numerical simulations and solid line represents the predictions of the standard kinetic theory [see Eq. (7)].

Individual components of the pressure tensor are shown in Figs. 2 and 3. According to the standard kinetic theory, the diagonal elements of the pressure tensor must be equal. As seen in Fig. 2, this is clearly not the case. The simulation results indicate much higher values for P_{22} compared with P_{11} and P_{33}. The differences are large especially near the walls. Nonequal diagonal components of the pressure tensor imply that the velocity variance is significantly anisotropic. Figure 3 compares the pressure component P_{12} obtained from the particle dynamics simulations with that predicted

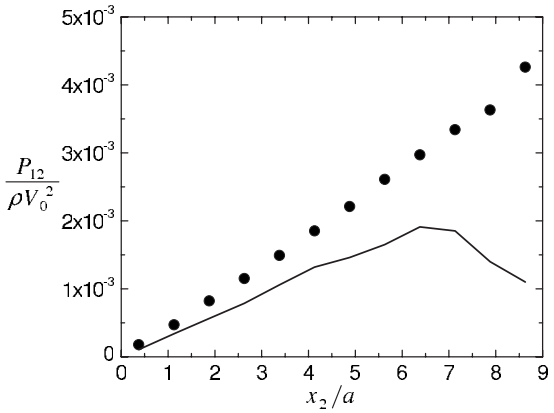

FIG. 3. Shear component of the pressure tensor. Filled circles: numerical simulations; line: standard kinetic theory [see Eq. (7)].

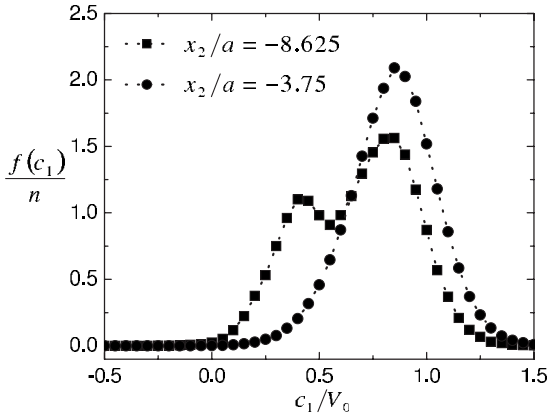

FIG. 4. The x_1-component velocity distribution at two different positions in the channel.

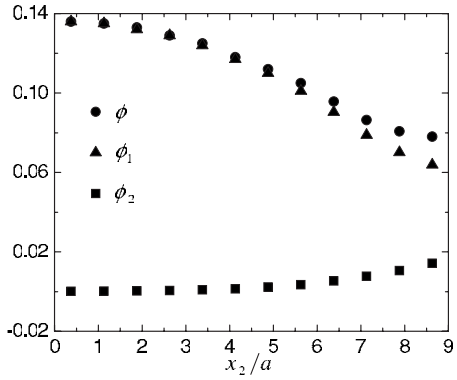

FIG. 6. Total and individual species volume fractions as functions of the position in the channel.

by the Newtonian rheology. We see significant differences between the two, once again near the walls.

Figures 4 and 5 show the velocity distributions for the c_1 and c_2 components at two different positions in the channel. We see that the velocity distribution is significantly bimodal near the walls. The smaller peak corresponds to the population of the particles that recently collided with the wall. Their velocity component parallel to the walls is considerably reduced as a result of that interaction. The majority of the particle population has a peak in the velocity that is close to the terminal velocity of the particles.

The results for the particle velocity distribution give us insight into why the simple kinetic theory based on the assumption of a nearly isotropic Maxwellian velocity distribution is inadequate for predicting the averaged equations of motion or the boundary conditions for the particulate suspension confined between two vertical rigid walls. The question we wish to address here is as follows: In a system such as this one, where the mean particle velocity is not small compared with the fluctuation velocities and where the mean free path a/ϕ is comparable to the half channel width (both of them equal to 10), can better agreement between the simulation results and a kinetic theory be obtained if the collision integrals are evaluated with greater accuracy? Several assumptions are typically made in evaluating the collision contribution to the particle phase pressure and rheology. Some of the assumptions may be relaxed if a more accurate velocity distribution of the particles is employed. The purpose of the present study is to carry out more accurate evaluation of the collision terms and then compare the results with those obtained from numerical simulations. In the process, we shall determine accurate closure relations and boundary conditions.

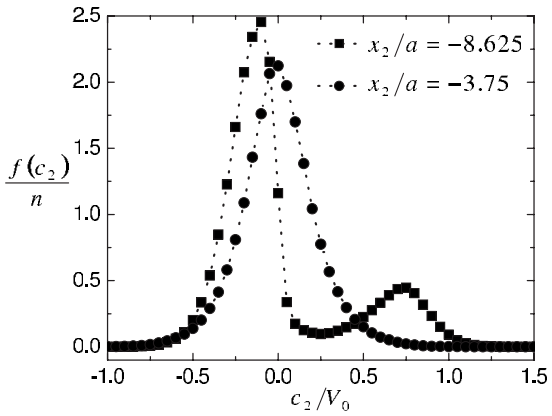

FIG. 5. The x_2-component velocity distribution at two different positions in the channel.

III. TWO-SPECIES KINETIC THEORY

In Sec. II we found that the velocity distribution for the monodisperse particulate system confined between two vertical rigid walls is bimodal and anisotropic when the particles lose momentum upon collision with a wall. We further showed that a simple kinetic theory is inadequate in describing the profiles of time-averaged velocity and volume fraction. To overcome some of these limitations, we have developed a more accurate kinetic theory that will account for both the bimodal and the anisotropic nature of the velocity distribution and carried out term-by-term comparison between the theory and simulations.

The bimodal nature of the velocity distribution is accounted for by treating the particulate system as consisting of two species: normal and wall excited, henceforth referred to as species 1 and 2, respectively. The latter are the particles whose most recent collision was with one of the channel walls. It is relatively straightforward in particle dynamics simulations to keep track of the particle collisions, and therefore the time-averaged volume fraction of each species can be easily determined. An example is shown in Fig. 6, which gives the volume fractions of each species for the case considered in Sec. II. We see that the volume fraction of the wall-excited species decreases away from the walls. In the present section we shall develop a kinetic theory that will allow us to predict the profiles for both species.

We treat particles of each species as rigid, elastic spheres having equal mass m and radius a. Note that for the case of a bubbly liquid, m may be taken as the average virtual mass of a bubble. The averaged mass, momentum, and energy equation for each species can be obtained from the general balance equation[41]

$$\frac{\partial}{\partial t}n_p\langle\psi^p\rangle + \frac{\partial}{\partial x_j}(n_p\langle c_j^p\psi^p\rangle) = n_p\left\langle\frac{F_j^p}{m}\cdot\frac{\partial\psi^p}{\partial c_j^p}\right\rangle + \sum_{q=1}^{2}\mathbf{C}^{p,q}(\psi), \tag{16}$$

where c_j^p is the velocity of the particles of species p, n_p an ensemble-averaged number density, F_j^p the sum of viscous and gravity forces acting on the particles, and $\mathbf{C}^{p,q}$ a collision operator for determining the contribution to the rate of change per unit volume in particle property ψ due to collisions. The angular brackets imply ensemble averaging of a quantity. Note that the species mass, momentum, and variance balance equations can be generated from the above expression by taking ψ^p equal to, respectively, m, $m\mathbf{c}^p$, and $\mathbf{c}^p\mathbf{c}^p$.

To evaluate $\mathbf{C}^{p,q}(\psi)$, we shall assume that only binary collisions occur. The usual kinetic theories of dense gas mixtures or granular materials account for the rate of change in ψ^p due to all possible collisions between the particles of species p and those of species q $(q=1,2)$. In our system, a collision of the particle of species 2 with another particle converts the particle of species 2 into 1 after the collision. Associated with this is a source term for species 1 and a sink term for species 2 for every collision involving species 2. We therefore express $\mathbf{C}^{p,q}(\psi)$ as a sum of two terms:

$$\mathbf{C}^{p,q}(\psi) = \mathbf{C}_+^{p,q}(\psi) + \mathbf{C}_*^{p,q}(\psi). \tag{17}$$

The first term on the rhs of Eq. (17) involves the change in the property during the collision, while the second gives the change in the property due to the conversion of particles of species 2. Thus, we write

$$\mathbf{C}_+^{p,q}(\psi) = \int_{\mathbf{g}\cdot\mathbf{k}>0}(\hat{\psi}^p - \psi^p)P^{p,q}(\mathbf{c}_1,\mathbf{r},\mathbf{c}_2,\mathbf{r}+\sigma^{p,q}\mathbf{k}) \times(\sigma^{p,q})^2(\mathbf{g}\cdot\mathbf{k})d\mathbf{k}d\mathbf{c}_1d\mathbf{c}_2 \tag{18}$$

and

$$\mathbf{C}_*^{p,q}(\psi) = (-1)^{p-1}\int_{\mathbf{g}\cdot\mathbf{k}>0}\hat{\psi}^2P^{2,q}(\mathbf{c}_1,\mathbf{r},\mathbf{c}_2,\mathbf{r}+\sigma^{2,q}\mathbf{k}) \times(\sigma^{2,q})^2(\mathbf{g}\cdot\mathbf{k})d\mathbf{k}d\mathbf{c}_1d\mathbf{c}_2. \tag{19}$$

Here, ψ^p and $\hat{\psi}^p$ are particle properties before and after a collision, $P^{p,q}(\mathbf{c}_1,\mathbf{r},\mathbf{c}_2,\mathbf{r}+\sigma^{p,q}\mathbf{k})$ is the pair probability distribution function for a particle of species p with velocity $\mathbf{c}_1$ at $\mathbf{r}$ and species q at $\mathbf{r}+\sigma^{p,q}\mathbf{k}$ with velocity $\mathbf{c}_2$, $\sigma^{p,q}=a^p+a^q$ is the center-to-center distance at the instance of a collision, a^p and a^q being the radii of particles of species p and q, $\mathbf{g}$ is the relative velocity of the particles just before the collision $(\mathbf{g}=\mathbf{c}_1-\mathbf{c}_2)$, and $\mathbf{k}$ is a unit vector directed from the center of the particle of species p to the center of the particle of species q at the instant of their contact. Note that, in general, while ψ^p is a function of $\mathbf{c}_1$, $\hat{\psi}^p$ is a function of both $\mathbf{c}_1$ and $\mathbf{c}_2$. The integrations in Eqs. (18) and (19) must be carried out for all possible values satisfying $\mathbf{g}\cdot\mathbf{k}>0$, which correspond to an impending collision. The factor $(-1)^{p-1}$ in Eq. (19) accounts for the conversion of species 2 into 1 after the collision.

$\mathbf{C}_+^{p,q}(\psi)$ and $\mathbf{C}_*^{p,q}(\psi)$ at the position $\mathbf{r}$ can be determined in a straightforward manner from numerical simulations by keeping track of collisions that occur in the vicinity of $\mathbf{r}$ and the resultant change in the particle property. For predicting their values in terms of some averaged quantities, kinetic theories typically make several simplifying assumptions. One common assumption is that the velocities of the two colliding particles are completely independent. The pair distribution function $P^{p,q}(\mathbf{c}_1,\mathbf{r},\mathbf{c}_2,\mathbf{r}+\sigma^{p,q}\mathbf{k})$ is expressed in terms of the product of two single particle velocity distribution functions $f^p(\mathbf{c}_1,\mathbf{r})$ and $f^q(\mathbf{c}_2,\mathbf{r}+\sigma^{p,q}\mathbf{k})$ as given by

$$P^{p,q}(\mathbf{c}_1,\mathbf{r},\mathbf{c}_2,\mathbf{r}+\sigma^{p,q}\mathbf{k}) = P_rf^p(\mathbf{c}_1,\mathbf{r})f^q(\mathbf{c}_2,\mathbf{r}+\sigma^{p,q}\mathbf{k}), \tag{20}$$

where P_r is a relative pair probability. In a macroscopically homogeneous system with an isotropic spatial pair probability distribution, it simply equals the radial distribution function for particles in contact and depends on the volume fraction of the particles. For inhomogeneous systems, a usual approximation is to take it equal to the radial distribution function at contact, corresponding to the average volume fraction of particles at the point halfway between the two particles.[26] Of course, in the present case, this relative probability also depends on the position of the pair of particles relative to the channel walls. However, we shall neglect that added complexity and simply take $P_r=G(\phi)$ with ϕ being evaluated at $\mathbf{r}+\sigma^{p,q}\mathbf{k}/2$, the point of contact of the two colliding particles, G being the radial distribution value for a hard-sphere configuration as given by Eq. (12). Next, it is assumed that the mean field variables vary slowly in space so that P_r and $f^q(\mathbf{c}_2,\mathbf{r}+\sigma^{p,q}\mathbf{k})$ may be expanded in Taylor series near point $\mathbf{r}$. Retaining terms up to $O(\sigma^{p,q}\mathbf{k})$, we obtain the following approximations for $\mathbf{C}_+^{p,q}(\psi)$ and $\mathbf{C}_*^{p,q}(\psi)$:

$$\mathbf{C}_+^{p,q}(\psi) = \chi^{p,q}(\psi) - \frac{\partial}{\partial x_j}\theta_j^{p,q}(\psi) \tag{21}$$

and

$$\mathbf{C}_*^{p,q}(\psi) = (-1)^{p-1}\left[S^{2,q}(\psi) - \frac{\partial}{\partial x_j}\hat{\theta}_j^{2,q}(\psi)\right]. \tag{22}$$

The two terms on the rhs of Eq. (21) will be referred to as the collisional source and flux for the rate of change in ψ^p and the two terms on the rhs of Eq. (22) as the source and flux due to the conversion of the wall-excited species into normal species. The source and flux terms in Eq. (21) are given by[29]

$$\chi^{p,q}(\psi) = (\sigma^{p,q})^2G[\phi(\mathbf{r})]\int_{\mathbf{g}\cdot\mathbf{k}>0}(\hat{\psi}^p - \psi^p)(\mathbf{g}\cdot\mathbf{k}) \times\left(1+\frac{\sigma^{p,q}}{2}\mathbf{k}\cdot\mathbf{D}^{p,q}\right)f^p(\mathbf{c}_1,\mathbf{r}) \times f^q(\mathbf{c}_2,\mathbf{r})d\mathbf{k}d\mathbf{c}_1d\mathbf{c}_2, \tag{23}$$

$$\theta_j^{p,q}(\psi) = -\frac{(\sigma^{p,q})^3}{2} G[\phi(\mathbf{r})] \int_{\mathbf{g}\cdot\mathbf{k}>0} (\hat{\psi}^p - \psi^p) k_j (\mathbf{g}\cdot\mathbf{k}) \times \left(1 + \frac{\sigma^{p,q}}{2}\mathbf{k}\cdot\mathbf{D}^{p,q}\right) f^p(\mathbf{c}_1,\mathbf{r}) \times f^q(\mathbf{c}_2,\mathbf{r}) d\mathbf{k} d\mathbf{c}_1 d\mathbf{c}_2, \tag{24}$$

where $\mathbf{D}^{p,q}$ is given by

$$D_k^{p,q} = \frac{\partial}{\partial x_k}\left(\ln\frac{f^q(\mathbf{c}_2,\mathbf{r})}{f^p(\mathbf{c}_1,\mathbf{r})}\right). \tag{25}$$

Expressions for the source and flux terms in Eq. (22) are obtained by replacing $(\hat{\psi}^p - \psi^p)$ in Eqs. (23) and (24) by $\hat{\psi}^2$ and setting $p=2$.

The integrals in the above expressions are typically evaluated by assuming that the single particle velocity distribution function $f^p(\mathbf{c}_1,\mathbf{r})$ deviates only slightly from the isotropic Maxwellian distribution (e.g., Grad approximation[25]). Since the velocity distribution in our system is considerably anisotropic, we assume an anisotropic Maxwellian:

$$f^p(\mathbf{c}_1,\mathbf{r}) = n_p \frac{\|\mathbf{A}^p\|^{1/2}}{(2\pi)^{3/2}} \exp\left[-\frac{1}{2}(\mathbf{c}_1 - \mathbf{V}^p)^T \mathbf{A}^p (\mathbf{c}_1 - \mathbf{V}^p)\right], \tag{26}$$

where n_p and $\mathbf{V}^p$ are, respectively, the number density and mean velocity of the particles, $\mathbf{A}^p$ is the inverse of the velocity variance tensor, $\mathbf{A}^p = (\mathbf{T}^p)^{-1}$ with $\|\mathbf{A}^p\| > 0$, and the superscript T stands for the transpose of a tensor. The vertical bars stand for the determinant of a tensor matrix.

The mass balance equations for the two species are obtained by substituting $\psi = m$ in Eq. (16). This yields

$$\frac{\partial(mn_p)}{\partial t} + \frac{\partial}{\partial x_j}(mn_p V_j^p) = \sum_{q=1}^{2} \mathbf{C}_*^{p,q}(m), \tag{27}$$

where the rhs stands for the source or sink term arising from the conversion of the wall-excited species. Equation (27) is exact. Our kinetic theory will obtain an approximation for the rhs of the above equation in terms of $S^{2,q}(m)$ and $\hat{\theta}_j^{2,q}(m)$ as given by Eq. (22) with $\psi = m$.

Similarly, the momentum equations are obtained by substituting $\psi^p = m\mathbf{c}^p$ in Eq. (16). After substituting the approximation for $\mathbf{C}_+^{p,q}(m\mathbf{c})$ from Eq. (21) and rearranging, we obtain the following approximate form of the momentum equations:

$$\frac{\partial}{\partial t}(mn_p V_i^p) + \frac{\partial}{\partial x_j}(mn_p V_i^p V_j^p + P_{ij}^p) = n_p(m_b \hat{g}_i - \lambda V_i^p) + \sum_{q=1}^{2} \chi^{p,q}(mc_i) + \sum_{q=1}^{2} \mathbf{C}_*^{p,q}(mc_i), \tag{28}$$

where the pressure tensor P_{ij}^p is given by

$$P_{ij}^p = mn_p \mathbf{T}_{ij}^p + \sum_{q=1}^{2} \theta_j^{p,q}(mc_i). \tag{29}$$

The first term on the rhs of the above equation represents the kinetic contribution to the pressure tensor and the second represents the collisional contribution. The total collisional pressure is given by

$$P_{ij}^{\mathrm{col}} = \sum_{p=1}^{2}\sum_{q=1}^{2} \theta_j^{p,q}(mc_i). \tag{30}$$

Note that the last term in Eq. (28) can be similarly approximated in terms of source and flux terms as in Eq. (22). We have not combined this flux term in the definition of the overall pressure tensor primarily so that we can compare the predictions of our theory with those presented in the literature for nonreacting bidisperse systems.

Finally, an approximate form of the balance equation for the second moments of the velocity fluctuations is given by

$$\frac{\partial}{\partial t}(mn_p \mathbf{T}_{ij}^p) + \frac{\partial}{\partial x_k}(mn_p V_k^p \mathbf{T}_{ij}^p + Q_{ijk}^p) = -2n_p \lambda \mathbf{T}_{ij}^p - \left(P_{jk}^p \frac{\partial V_i^p}{\partial x_k} + P_{ik}^p \frac{\partial V_j^p}{\partial x_k}\right) + \sum_{q=1}^{2} \Gamma_{ij}^{p,q} + \sum_{q=1}^{2} \hat{\Gamma}_{ij}^{p,q}, \tag{31}$$

where the heat flux tensor, given by

$$Q_{ijk}^p = mn_p \langle C_i^p C_j^p C_k^p \rangle + \sum_{q=1}^{2} \theta_k^{p,q}(mC_i C_j), \tag{32}$$

consists of the usual kinetic and collisional contributions. (Note that the heat flux vector q_j introduced in Sec. II is related to the heat flux tensor defined here by $q_j = 2\Sigma_{p=1}^{2} Q_{iij}^p$.) The first term on the rhs of Eq. (31) represents the viscous dissipation, and the second and third terms represent the production of fluctuation energy due to P_{ij}^p acting on the velocity gradient. $\Gamma_{ij}^{p,q}$ is the collisional source of fluctuations $[\Gamma_{ij}^{p,q} = \chi^{p,q}(mC_iC_j)]$ and

$$\hat{\Gamma}_{ij}^{p,q} = \mathbf{C}_*^{p,q}(mc_ic_j) - V_i^p \mathbf{C}_*^{p,q}(mc_j) - V_j^p \mathbf{C}_*^{p,q}(mc_i) + V_i^p V_j^p \mathbf{C}_*^{p,q}(m). \tag{33}$$

The balance equations given by Eqs. (27), (28), and (31) must be supplemented with appropriate boundary conditions and closure relations for the flux of velocity fluctuations. Before introducing these elements, we first verify the accuracy of the kinetic theory by calculating various terms in the balance equations using the values of ϕ_p, $\mathbf{V}^p$, and $\mathbf{T}^p$ obtained in numerical simulations and carry out term-by-term comparison of the predictions of kinetic theory with the results of numerical simulations. In this manner we can identify any source of discrepancy between the simulations and the theory and analyze the reasons for the discrepancy. Also, this term-by-term comparison will aid in developing and assessing closure relations for various terms appearing in the balance equations. The results of this detailed comparison

will be presented in Sec. IV. In the remainder of this section, we give the details of the technique used for determining various collision integrals accurately. Expressions will be given in Sec. IV and Appendix B for the limiting case when the relative velocity of the two species is large compared with the root-mean-squared velocity fluctuations.

A. Calculation of collision integrals

Calculation of the collision integrals is facilitated by carrying out change in variables from $\mathbf{c}_1$ and $\mathbf{c}_2$ to $\mathbf{g}=\mathbf{c}_1-\mathbf{c}_2$ and $\mathbf{c}'=\frac{1}{2}(\mathbf{c}_1+\mathbf{c}_2)$. The Jacobian of the transformation of variables from $\mathbf{c}_1$ and $\mathbf{c}_2$ to $\mathbf{g}$ and $\mathbf{c}'$ is unity. We then express the product of single particle velocity distribution functions $f^p(\mathbf{c}_1,\mathbf{r})f^q(\mathbf{c}_2,\mathbf{r})$ and $\mathbf{D}^{p,q}$ in terms of $\mathbf{g}$ and $\mathbf{c}'$. We first carry out integration over $\mathbf{k}$ and then over $\mathbf{c}'$. Both these integrations are performed analytically whereas the integration over $\mathbf{g}$ is performed numerically. Tables of integrals given by Chapman and Cowling[24] and Jenkins and Richman[25] are useful for carrying out the analytical integration over $\mathbf{k}$. Details of the analytical integration over $\mathbf{c}'$ and numerical integration over $\mathbf{g}$ are given below where we outline the calculation of the collisional source of momentum.

Using Eq. (26), we write the product $f^p(\mathbf{c}_1,\mathbf{r})f^q(\mathbf{c}_2,\mathbf{r})$ as

$$f^p(\mathbf{c}_1,\mathbf{r})f^q(\mathbf{c}_2,\mathbf{r}) = \Omega^{p,(0)}\Omega^{q,(0)}\exp\left(-\tfrac{1}{2}B\right), \tag{34}$$

where

$$\Omega^{p,(0)} = n_p\|\mathbf{A}^p\|^{1/2}/(2\pi)^{3/2}, \quad \Omega^{q,(0)} = n_q\|\mathbf{A}^q\|^{1/2}/(2\pi)^{3/2}, \tag{35}$$

and

$$B = (\mathbf{c}_1-\mathbf{V}^p)^T\mathbf{A}^p(\mathbf{c}_1-\mathbf{V}^p) + (\mathbf{c}_2-\mathbf{V}^q)^T\mathbf{A}^q(\mathbf{c}_2-\mathbf{V}^q). \tag{36}$$

Substituting expressions for $\mathbf{c}_1$ and $\mathbf{c}_2$ in terms of $\mathbf{c}'$ and $\mathbf{g}$ in Eq. (36) and after some rearranging, we obtain

$$B = (\mathbf{g}-\Delta\mathbf{V}^{p,q})^T\mathbf{B}^{p,q}(\mathbf{g}-\Delta\mathbf{V}^{p,q}) + (\mathbf{c}'-\mathbf{W}^{p,q})^T\mathbf{A}^{p,q}(\mathbf{c}'-\mathbf{W}^{p,q}), \tag{37}$$

where

$$\mathbf{A}^{p,q} = \mathbf{A}^p + \mathbf{A}^q, \quad \mathbf{B}^{p,q} = (\mathbf{T}^p+\mathbf{T}^q)^{-1}, \quad \Delta\mathbf{V}^{p,q} = \mathbf{V}^p - \mathbf{V}^q, \tag{38}$$

and

$$\mathbf{W}^{p,q} = (\mathbf{A}^{p,q})^{-1}(\mathbf{A}^p\mathbf{V}^p + \mathbf{A}^q\mathbf{V}^q) + \tfrac{1}{2}(\mathbf{T}^p-\mathbf{T}^q)\mathbf{B}^{p,q}\mathbf{g}. \tag{39}$$

Upon substituting the expression for B given by Eq. (37) into Eq. (34), we obtain

$$f^p(\mathbf{c}_1,\mathbf{r})f^q(\mathbf{c}_2,\mathbf{r}) = \Omega^{p,(0)}\Omega^{q,(0)}E_1(\mathbf{c}',\mathbf{g})E_2(\mathbf{g}), \tag{40}$$

where $E_1(\mathbf{c}',\mathbf{g})$ and $E_2(\mathbf{g})$ are given by

$$E_1(\mathbf{c}',\mathbf{g}) = \exp\left[-\tfrac{1}{2}(\mathbf{c}'-\mathbf{W}^{p,q})^T\mathbf{A}^{p,q}(\mathbf{c}'-\mathbf{W}^{p,q})\right], \tag{41}$$

$$E_2(\mathbf{g}) = \exp\left[-\tfrac{1}{2}(\mathbf{g}-\Delta\mathbf{V}^{p,q})^T\mathbf{B}^{p,q}(\mathbf{g}-\Delta\mathbf{V}^{p,q})\right]. \tag{42}$$

Next, we express $\mathbf{D}^{p,q}$ in terms of $\mathbf{c}'$ and $\mathbf{g}$. Substituting single particle velocity distribution functions given by Eq. (26) into Eq. (25), using the expressions for $\mathbf{c}_1$ and $\mathbf{c}_2$ in terms of $\mathbf{c}'$ and $\mathbf{g}$, and expanding, we obtain

$$\begin{aligned} D_k^{p,q} = {} & \frac{\partial}{\partial x_k}\left(\ln\frac{\Omega^{q,(0)}}{\Omega^{p,(0)}}\right) + \frac{1}{2}(c_i' + g_i/2 - V_i^p)(c_j' + g_j/2 - V_j^p) \\ & \times\frac{\partial}{\partial x_k}(\mathbf{A}_{ij}^p) - \frac{1}{2}(c_i' - g_i/2 - V_i^q)(c_j' - g_j/2 - V_j^q) \\ & \times\frac{\partial}{\partial x_k}(\mathbf{A}_{ij}^q) - \mathbf{A}_{ij}^p(c_j' + g_j/2 - V_j^p)\frac{\partial}{\partial x_k}(V_i^p) \\ & + \mathbf{A}_{ij}^q(c_j' - g_j/2 - V_j^q)\frac{\partial}{\partial x_k}(V_i^q). \end{aligned} \tag{43}$$

The above expression for $D_k^{p,q}$ is rearranged as

$$D_k^{p,q} = d_k^0 + d_{ki}^1 c_i' + d_{kij}^2 c_i' c_j', \tag{44}$$

with

$$\begin{aligned} d_k^0 = {} & \frac{\partial}{\partial x_k}\left(\ln\frac{\Omega^{q,(0)}}{\Omega^{p,(0)}}\right) - \mathbf{A}_{ij}^p(g_j/2 - V_j^p)\frac{\partial}{\partial x_k}(V_i^p) \\ & + \frac{1}{2}(g_i/2 - V_i^p)(g_j/2 - V_j^p)\frac{\partial}{\partial x_k}(\mathbf{A}_{ij}^p) - \mathbf{A}_{ij}^q(g_j/2 + V_j^q) \\ & \times\frac{\partial}{\partial x_k}(V_i^q) - \frac{1}{2}(g_i/2 + V_i^q)(g_j/2 + V_j^q)\frac{\partial}{\partial x_k}(\mathbf{A}_{ij}^q), \end{aligned} \tag{45}$$

$$\begin{aligned} d_{ki}^1 = {} & (g_j/2 - V_j^p)\frac{\partial}{\partial x_k}(\mathbf{A}_{ij}^p) - \mathbf{A}_{ij}^p\frac{\partial}{\partial x_k}(V_j^p) \\ & + (g_j/2 + V_j^q)\frac{\partial}{\partial x_k}(\mathbf{A}_{ij}^q) + \mathbf{A}_{ij}^q\frac{\partial}{\partial x_k}(V_j^q), \end{aligned} \tag{46}$$

and

$$d_{kij}^2 = \frac{1}{2}\left(\frac{\partial}{\partial x_k}(\mathbf{A}_{ij}^p) - \frac{\partial}{\partial x_k}(\mathbf{A}_{ij}^q)\right). \tag{47}$$

To evaluate the collisional source of momentum $\chi^{p,q}(m\mathbf{c})$, we substitute $\psi=m\mathbf{c}$ in Eq. (23). The term $(\hat{\psi}^p-\psi^p)$, which now represents the change in the momentum of the particle of species p in a collision, is given by

$$(\hat{\psi}^p - \psi^p) = m(\hat{\mathbf{c}}^p - \mathbf{c}^p) = -m(\mathbf{g}\cdot\mathbf{k})\mathbf{k}. \tag{48}$$

Substituting Eqs. (40) and (48) into Eq. (23), the collisional source of momentum is expressed as

$$\chi^{p,q}(m\mathbf{c}) = -(\sigma^{p,q})^2 G\Omega^{p,(0)}\Omega^{q,(0)}m \times\int I_m\mathbf{k}(\mathbf{g}\cdot\mathbf{k})^2E_2(\mathbf{g})d\mathbf{k}d\mathbf{g}, \tag{49}$$

where I_m is given by

$$I_m = \int\left(1 + \frac{\sigma^{p,q}}{2}\mathbf{k}\cdot\mathbf{D}^{p,q}\right)E_1(\mathbf{c}',\mathbf{g})d\mathbf{c}'. \tag{50}$$

To perform the analytical integration over $\mathbf{c}'$, we substitute the expressions for $E_1(\mathbf{c}',\mathbf{g})$ and $\mathbf{D}^{p,q}$ given by Eqs. (41) and (44) into Eq. (50). Using the integration formulas given in Appendix A, we obtain

$$I_m = \Omega^{p,q,(1)}\left(1 + \frac{\sigma^{p,q}}{2}\mathbf{k}\cdot\mathbf{\Lambda}\right), \tag{51}$$

where

$$\Lambda_k = d_k^0 + d_{ki}^1 W_i^{p,q} + d_{kij}^2 (W_i^{p,q} W_j^{p,q} + \mathbf{T}_{ij}^m). \tag{52}$$

Substituting I_m given by Eq. (51) into Eq. (49) and integrating over $\mathbf{k}$ using the formulas given by Jenkins and Richman,[25] we obtain

$$\chi^{p,q}(m\mathbf{c}) = \omega^{p,q}\int F(\mathbf{g})E_2(\mathbf{g})d\mathbf{g}, \tag{53}$$

where

$$F(\mathbf{g}) = \left\{\frac{|g|}{2}\mathbf{g} + \frac{\sigma^{p,q}}{15}[2\mathbf{g}(\mathbf{\Lambda}\cdot\mathbf{g}) + |g|^2\mathbf{\Lambda}]\right\} \tag{54}$$

and $\omega^{p,q} = -(\sigma^{p,q})^2 G\Omega^{p,(0)}\Omega^{q,(0)}\Omega^{p,q,(1)}m$. In Eq. (54), $|g|$ is the magnitude of $\mathbf{g}$. The remaining integration over $\mathbf{g}$ is carried out numerically. For this purpose, we first write

$$\mathbf{g} = \Delta\mathbf{V}^{p,q} + \mathbf{R}\cdot\mathbf{u}, \tag{55}$$

where the matrix $\mathbf{R}$ is related to the eigenvectors and eigenvalues of $\mathbf{B}^{p,q}$:

$$R = \begin{bmatrix} \cos\zeta/\sqrt{\beta_1} & \sin\zeta/\sqrt{\beta_2} & 0 \\ -\sin\zeta/\sqrt{\beta_1} & \cos\zeta/\sqrt{\beta_2} & 0 \\ 0 & 0 & 1/\sqrt{\beta_3} \end{bmatrix}. \tag{56}$$

Here, $\zeta = \frac{1}{2}\tan^{-1}[2B_{12}^{p,q}/(B_{22}^{p,q} - B_{11}^{p,q})]$ and β_1, β_2, and β_3 are the eigenvalues of $\mathbf{B}^{p,q}$:

$$\begin{aligned} \beta_1 &= B_{11}^{p,q}\cos^2\zeta + B_{22}^{p,q}\sin^2\zeta - B_{12}^{p,q}\sin 2\zeta, \\ \beta_2 &= B_{22}^{p,q}\cos^2\zeta + B_{11}^{p,q}\sin^2\zeta + B_{12}^{p,q}\sin 2\zeta, \\ \beta_3 &= B_{33}^{p,q}. \end{aligned} \tag{57}$$

The Jacobian of the transformation given by Eq. (55) is $\beta = (\beta_1\beta_2\beta_3)^{-1/2}$. Carrying out the transformation from (u_1, u_2, u_3) to spherical coordinates (s, ξ, φ) in Eq. (53), we obtain

$$\chi^{p,q}(m\mathbf{c}) = \omega^{p,q}\beta\int_0^{2\pi}\int_0^{\pi}\int_0^{\infty} F(s,\xi,\varphi) \times\exp\left(-\frac{s^2}{2}\right)s^2\sin\xi ds d\xi d\varphi. \tag{58}$$

The above integrations over s, ξ, and φ were performed numerically using a 12-point Gaussian quadrature for the integrations over ξ and φ and Simpson's rule with 81 points between $s=2$ and 10 for the integration over s.

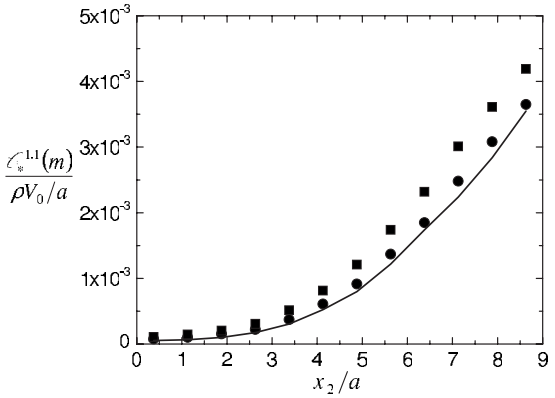

FIG. 7. The results for the source term $\mathbf{C}_*^{1,1}(m)$. Numerical simulations: filled circles; kinetic theory: solid line. The filled squares represent the contribution of the source term $S^{2,1}(m)$ to $\mathbf{C}_*^{1,1}(m)$.

IV. RESULTS

A. Verification of the balance equations and closure relations

We begin with the mass conservation equation for species 1. The results are presented in the dimensionless form by normalizing $\mathbf{V}^p$ and $(\mathbf{T}^p)^{1/2}$ with particle terminal velocity V_0, x_2 by particle radius a, and t by a/V_0. We first verify the overall mass conservation equation. The lhs and rhs of Eq. (27) were each determined separately from the results of numerical simulations. The lhs, which represents the derivative of $\phi_1 V_2^1$ with respect to x_2, was determined using the central difference formula for all points except those near the walls, where a three-point backward or forward difference was used. The derivatives thus computed were compared with the sum of the source terms, $\mathbf{C}_*^{1,1}(m) + \mathbf{C}_*^{1,2}(m)$, determined from numerical simulations. The two agreed with each other nearly perfectly at all points, thus validating the mass conservation equation.

We now compare the simulation results with the predictions of the kinetic theory. Recall that the source $\mathbf{C}_*^{1,q}(m)$ is approximated in the kinetic theory in terms of two terms, $S^{2,q}$ and the x_2 derivative of $\hat{\theta}_2^{2,q}$ [see Eq. (22)]. The solid line in Fig. 7 shows the predicted values of $\mathbf{C}_*^{1,1}(m)$. To determine these values, we used ϕ_p, $\mathbf{V}^p$, and $\mathbf{T}^p$ obtained from simulations and evaluated the collision integrals in Eq. (22) as described in detail in Sec. III. The filled circles in Fig. 7 represent the values of $\mathbf{C}_*^{1,1}(m)$ determined from numerical simulations. We see that the two agree at all points including those closest to the walls, indicating that the kinetic theory provides an excellent approximation for the source term when ϕ_p, $\mathbf{V}^p$, and $\mathbf{T}^p$ are known exactly. The filled squares in Fig. 7 represent the contribution to $\mathbf{C}_*^{1,1}(m)$ from the source term $S^{2,1}$ in Eq. (22). We note that in this case the contribution from the flux term is maximum near the walls where it accounts for roughly 10% of the overall source.

The detailed computations for the source and flux terms using the kinetic theory described in Sec. III are somewhat involved and it is desirable to compare the results with those predicted using simpler kinetic theories. In particular, we shall be interested in the two limiting theories. The first as-

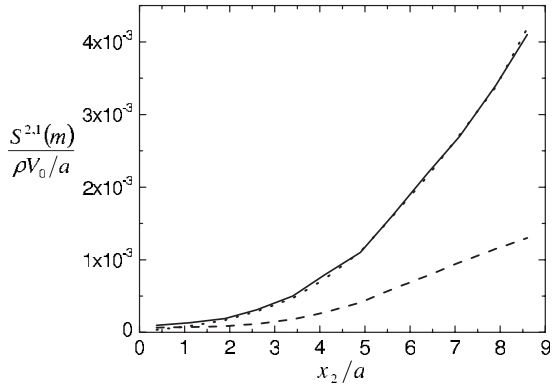

FIG. 8. Predictions of the mass source term $S^{2,1}(m)$ from detailed kinetic theory (solid line) and two limiting theories. The dashed line represents a theory which assumes simple isotropic Maxwellian velocity distributions for both species and the dotted line (almost indistinguishable from the solid line) represents a theory which assumes that both species are moving simply with their average velocities (LV approximation).

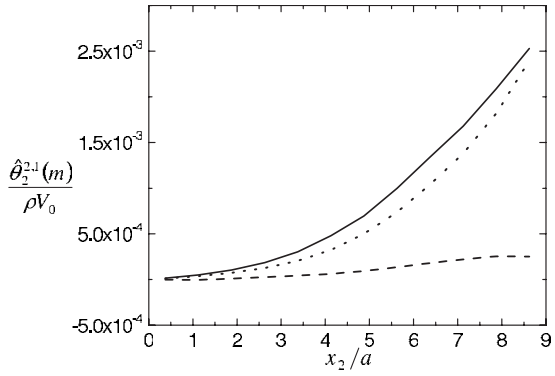

FIG. 9. The predictions of the mass flux term $\hat{\theta}_2^{2,1}(m)$ from the detailed kinetic theory (solid line) and two the limiting theories (dotted line: LV approximation; dashed line: SV approximation).

sumes a simple velocity distribution in which the velocity distributions of both species are assumed to be given by isotropic Maxwellians with their corresponding temperatures determined from the simulations and the mean relative velocities of the species being negligible, and the other assumes that both species are moving simply with their respective average velocities, i.e., their temperatures are negligibly small. These will be referred to, respectively, as SV (small relative velocity) and LV (large relative velocity) approximations. To obtain the predictions for these two limiting cases, we used our computer program for the general case. The LV approximation was obtained by simply multiplying the temperatures by a small number, typically 10^{-6}, and similarly, the SV approximation was obtained by multiplying the mean velocities by a small number and setting $\mathbf{T}_{ij}^{p}=\mathbf{T}^{p}\delta_{ij}$. Analytical expressions for the LV case were also obtained, and they are given below as needed.

The predictions of these two simple theories for the source term are compared against those determined from the detailed kinetic theory in Fig. 8. We see that the simpler theory based on the assumption that the two species are simply moving with their average velocities (LV approximation) gives very accurate estimates of the source term. Thus, the source term in the present case may be approximated by

$$S^{2,q}(m) = (\sigma^{2,q})^2 Gm\pi\left[n_2 n_q |\mathbf{V}^2 - \mathbf{V}^q| + \frac{\sigma^{2,q}}{2}\left(n_2 \frac{\partial n_q}{\partial x_j} - n_q \frac{\partial n_2}{\partial x_j}\right)(V_j^2 - V_j^q)\right]. \tag{59}$$

The results for the mass flux terms are similarly shown in Fig. 9, where, once again, we see that the results of the detailed kinetic theory can be reasonably well reproduced with a simpler theory based on LV approximation, which gives

$$\hat{\theta}_j^{2,q}(m) = -\frac{(\sigma^{2,q})^3}{2} Gm\pi n_2 n_q (V_j^2 - V_j^q). \tag{60}$$

In evaluating the above flux term, we have neglected the $\mathbf{k}\cdot\mathbf{D}^{p,q}$ term in Eq. (24) which would have given additional terms involving derivatives of the number density.

We now consider the momentum equation. The lhs and rhs of Eq. (28) are shown by, respectively, filled circles and the dashed line in Fig. 10. Once again, we see very good agreement, indicating the validity of the averaged momentum equation. Figure 10 also shows the three individual terms on the rhs of Eq. (28). We see that the rhs is dominated by the source term due to conversion, viz., $\mathbf{C}_*^{1,q}(mc_1)$, except very close to the channel center. Interestingly, the term $\phi_1(1-V_1^1)$ is seen to be approximately constant throughout most of the channel width. This suggests that $\phi_1 V_1^1$ is approximately constant. From the continuity equation, it is easy to see that actually this term is related to the source term $\mathbf{C}_*^{1,q}(m)$, the magnitude of which, being $O(\phi^2)$, is small for the case considered here.

Figure 11 shows a comparison between the results for the source of momentum due to species conversion $\mathbf{C}_*^{1,1}(mc_1)+\mathbf{C}_*^{1,2}(mc_1)$ obtained using the detailed kinetic theory with that from a simpler LV approximation. We see

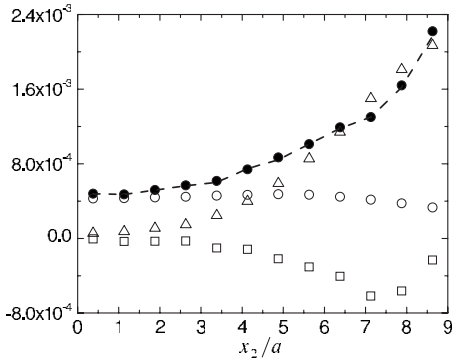

FIG. 10. Momentum balance for species 1. Filled circles and dashed line represent, respectively, the lhs and rhs of the momentum equation [see Eq. (28)]. Open circles represent the first term on the rhs of Eq. (28); open squares and triangles represent, respectively, the second and third terms on the rhs of the same equation.

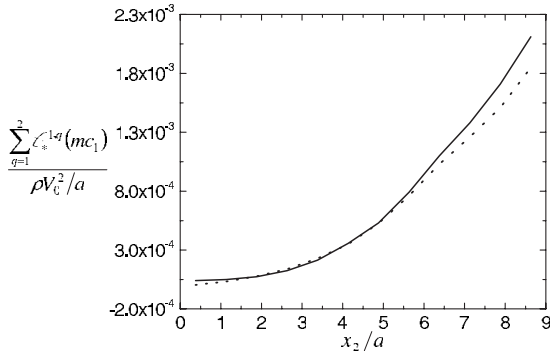

FIG. 11. A comparison of the momentum source due to conversion of species obtained using the detailed kinetic theory (solid line) with the limiting theory (dotted line) which assumes that both species are moving simply with their average velocities (LV approximation).

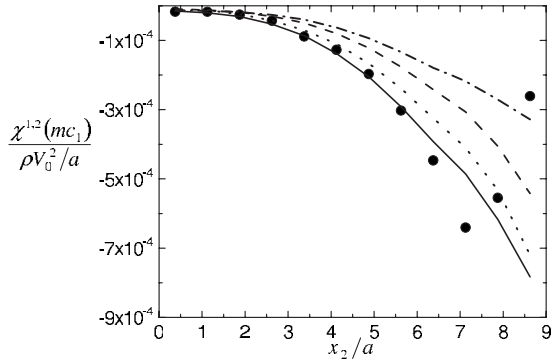

FIG. 12. Results for the source of momentum in the absence of mass exchange, i.e., $\chi^{1,2}(mc_1)$. Filled circles: numerical simulations; solid line: detailed kinetic theory; dotted line: LV approximation; dashed line: Jenkins and Mancini (Ref. 26) theory; dashed-dotted line: Lathouwers and Bellan (Ref. 33) theory.

that the simpler theory gives very accurate estimates. It may be noted that the other limiting theory, which assumes that the mean velocities of the two species are zero, will yield vanishing values for the source. Thus, the source and flux terms in the momentum equation can be determined using the following expressions based on the LV approximation:

$$S^{2,q}(mc_i) = (\sigma^{2,q})^2 Gm\pi\left\{ V_i^2\left[n_2 n_q |\mathbf{V}^2 - \mathbf{V}^q| + \frac{\sigma^{2,q}}{3}(V_j^2 - V_j^q)\left(n_2 \frac{\partial n_q}{\partial x_j} - n_q \frac{\partial n_2}{\partial x_j} \right) \right] - \frac{1}{2} n_2 n_q (V_i^2 - V_i^q)|\mathbf{V}^2 - \mathbf{V}^q| - \frac{\sigma^{2,q}}{15}\left(n_2 \frac{\partial n_q}{\partial x_j} - n_q \frac{\partial n_2}{\partial x_j} \right) \times [2(V_i^2 - V_i^q)(V_j^2 - V_j^q) + \delta_{ij}|\mathbf{V}^2 - \mathbf{V}^q|^2] \right\}, \tag{61}$$

$$\hat{\theta}_j^{2,q}(mc_i) = -\frac{(\sigma^{2,q})^3}{2} n_2 n_q Gm\pi\left\{ \frac{2}{3} V_i^2 (V_j^2 - V_j^q) - \frac{2}{15}[2(V_i^2 - V_i^q)(V_j^2 - V_j^q) + \delta_{ij}|\mathbf{V}^2 - \mathbf{V}^q|^2] \right\}. \tag{62}$$

Next, we consider the source of momentum in the absence of mass exchange, i.e., $\chi^{1,2}(mc_1)$ for a nonreacting mixture. The solid line in Fig. 12 shows the results obtained using the detailed kinetic theory. The simulation results are indicated by closed circles. The latter were obtained from the particle dynamics simulations, which actually yield $\mathbf{C}_+^{1,2}(mc_1)$. They were corrected by adding the flux term [see Eq. (21)] estimated from the simulation results. We see good agreement at all points except for a couple of points near the walls. The reason for the discrepancy between the theory and simulation results near the walls is unknown. There are at least two possible sources for the discrepancy. First, our theory assumes that all orientations of the colliding pairs of particles are equally probable. This is most likely not the case near the channel walls. Second, our assumption of anisotropic Maxwellian velocity distribution for the two species cannot be strictly justified for particles near the walls where, for example, the distribution predicts a finite, nonzero probability for wall-excited particles to have motion toward the wall.

Also shown in Fig. 12 are the predictions based on several simpler kinetic theories. The dashed line represents the predictions based on the expression given by Jenkins and Mancini,[26]

$$\chi^{p,q}(mc_i) = n_p n_q G(\sigma^{p,q})^2\left[\frac{2\pi}{3}\sigma^{p,q} T^{\mathrm{JM}} \frac{\partial}{\partial x_i}\left(\ln\frac{n_p}{n_q} \right) + \frac{8}{3}(\pi m T^{\mathrm{JM}})^{1/2}(V_i^q - V_i^p) \right], \tag{63}$$

where

$$T^{\mathrm{JM}} = (n_1 T^{\mathrm{JM},1} + n_2 T^{\mathrm{JM},2})/(n_1 + n_2), \tag{64}$$

$$T^{\mathrm{JM},p} = \frac{m}{3}\left\langle \left(\mathbf{c}^p - \frac{n_1\mathbf{V}^1 + n_2\mathbf{V}^2}{n_1 + n_2} \right) \cdot \left(\mathbf{c}^p - \frac{n_1\mathbf{V}^1 + n_2\mathbf{V}^2}{n_1 + n_2} \right) \right\rangle. \tag{65}$$

Lathouwers and Bellan[33] proposed

$$\chi^{p,q}(mc_i) = n_p n_q m G(\sigma^{p,q})^2\left[\frac{\pi}{3}\sigma^{p,q}(T^p + T^q)\frac{\partial}{\partial x_i}\left(\ln\frac{n_p}{n_q} \right) + \frac{4}{3}(2\pi)^{1/2}(T^p + T^q)^{1/2}(V_i^q - V_i^p) \right]. \tag{66}$$

As seen in Fig. 12, both closure relations yield poor estimates of the momentum source. Figure 12 also shows the results obtained by the LV theory which yields

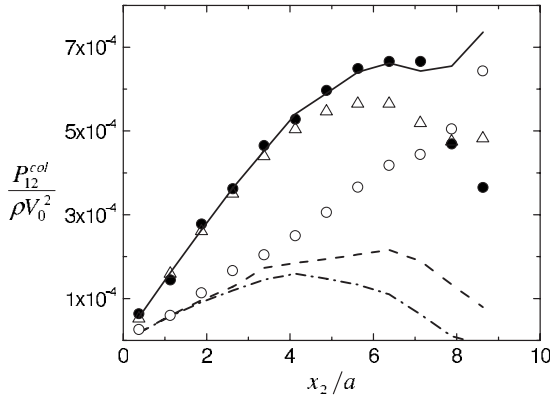

FIG. 13. Results for the total collisional contribution to the shear component P_{12}^{col} [see Eq. (30)]. Filled circles: numerical simulations; solid line: detailed kinetic theory; dashed line: Jenkins and Mancini (Ref. 28) theory; dashed-dotted line: Lathouwers and Bellan (Ref. 33) theory; open circles: LV approximation added to the Jenkins and Mancini theory, triangles: Grad approximation added to the results given by open circles.

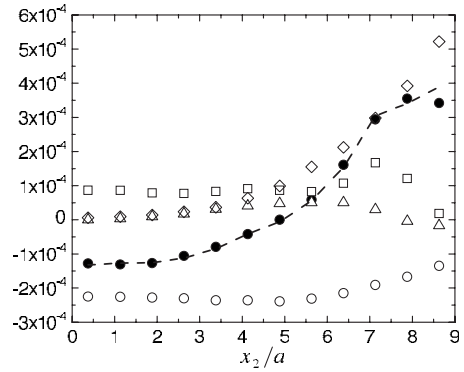

FIG. 14. Filled circles and dashed line represent, respectively, the lhs and rhs of the balance equation [see Eq. (31)] for $\mathbf{T}_{11}^{1}$. Open symbols represent various terms on the rhs of Eq. (31). Circles represent the first term, squares the second and third terms, triangles the fourth term, and diamonds the fifth term.

$$\chi^{p,q}(mc_i) = -(\sigma^{p,q})^2 Gm\pi\left\{\frac{1}{2}n_p n_q(V_i^p - V_i^q)|\mathbf{V}^p - \mathbf{V}^q| + \frac{\sigma^{p,q}}{15}[2(V_i^p - V_i^q)(V_j^p - V_j^q) + \delta_{ij}|\mathbf{V}^p - \mathbf{V}^q|^2]\left(n_p\frac{\partial n_q}{\partial x_j} - n_q\frac{\partial n_p}{\partial x_j}\right)\right\}. \tag{67}$$

We see that the predictions based on this simple theory are in good agreement with the results of more detailed kinetic theory.

Next, we present results for the total collisional contribution to the pressure tensor, i.e., P_{12}^{col} [see Eq. (30)]. As seen in Fig. 13, once again the simulation results are in good agreement with those determined using the detailed kinetic theory except very close to the wall. The predictions based on the expressions given by Jenkins and Mancini[28] and by Lathouwers and Bellan[33] are also shown in the figure. We see that both theories give significantly lower magnitudes of the collisional contribution P_{12}^{col}. Since these theories are derived for the rapidly sheared materials for which the root-mean-squared velocities are large compared with the mean velocities, it is not surprising that the agreement between these theories and simulations is not very good. The open circles in Fig. 13 indicate the predictions obtained from a simple theory in which the collisional contributions obtained by assuming that the particles of the two species are moving with their average velocities (LV approximation) are added to the closure relation suggested by Jenkins and Mancini.[28] We see that this results in some improvement but still falls short of predicting accurately the total collisional contribution to P_{12}^{col}. The discrepancy must therefore be related to the anisotropic nature of the velocity variance. A simpler way to account for the anisotropy is to use the Grad approximation which assumes a small perturbation to the isotropic Maxwellian velocity distribution. The resulting expression is given by

$$P_{12}^{\mathrm{col}} = \sum_{q=1}^{2}(8/5)mn_p\phi_p G\mathbf{T}_{12}^{p} + P_{12}^{\mathrm{LV}} + P_{12}^{\mathrm{JM}}. \tag{68}$$

The first term on the rhs of the above equation obtained using the Grad approximation requires knowledge of $\mathbf{T}_{12}^{p}$. The second term is obtained from the LV approximation [see Eq. (B2)] while the third is obtained using the closure relation proposed by Jenkins and Mancini[28] [Eqs. (36)–(39) in their paper]. The resulting prediction, shown by triangles in Fig. 13, is in excellent agreement with the results of particle dynamics simulations.

We now consider the balance equation for the second moments of the velocity fluctuations. The lhs and rhs of Eq. (31) for the balance of $\mathbf{T}_{11}^{1}$ are shown by, respectively, closed circles and dashed line in Fig. 14. We see that the two are in perfect agreement except for the point closest to the wall. The figure also shows contributions from the five terms on the rhs of the equation. Note that all terms play significant roles in the balance, especially near the wall.

The source terms $\hat{\Gamma}_{ij}^{p,q}$ and $\Gamma_{ij}^{p,q}$ computed from numerical simulations were compared with those predicted using the kinetic theory. The agreement was found to be generally good although not as good as for the source terms in the mass and momentum equations. Once again, significant deviations were observed between the predictions based on simple constitutive relations for bidisperse systems by Jenkins and Mancini[26] and the simulation results.

Perhaps the most difficult part is the prediction of Q_{ijk}^{p} for which we found that both the kinetic and collisional contributions are comparable in magnitude for the case considered in Sec. II. The collisional part is generally not well predicted by the theory while the kinetic part requires a closure relation. We have been unable to obtain a closure relation that adequately fits the results of particle dynamics simulations. The simplest closure relation is

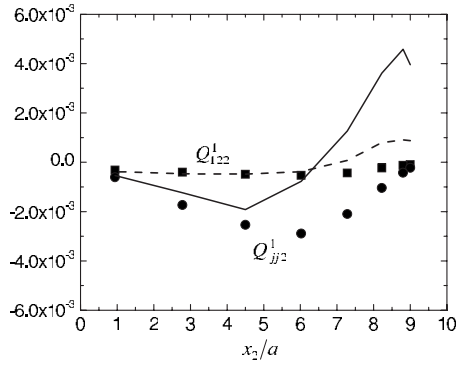

FIG. 15. Two selected components of heat flux tensor (Q^1_{122} and Q^1_{jj2}). Symbols represent results from numerical simulations and lines represent predictions by the closure relation given by Eq. (69).

$$Q^p_{ijk} = -(2/5)k(T^p,\phi)\left(\frac{\partial \mathbf{T}^p_{ij}}{\partial x_k} + \frac{\partial \mathbf{T}^p_{ik}}{\partial x_j} + \frac{\partial \mathbf{T}^p_{jk}}{\partial x_i}\right) + \sum_{q=1}^{2} \theta^{p,q}_k (mC_iC_j), \tag{69}$$

where k is given by the dense gas conductivity expression, Eq. (11), and the last term on the rhs is to be evaluated using the LV approximation. Note that the above reduces to $Q_{jjk} = 2q_k$ used in the simple theory described in Sec. II for the special case of an isotropic velocity variance. Figure 15 shows a comparison between the results obtained from particle dynamics simulations and the above closure relation for two selected components of the heat flux tensor (Q^1_{122} and Q^1_{jj2}). We note significant discrepancy, especially near the walls. Adding to the above expression for Q_{jjk}, a term suggested by Jenkins and Mancini[26] produces no significant improvement. Interestingly, we found that most heat flux components for species 1 have values close to zero near the walls where the temperature gradients are generally significant. Thus closure relations involving gradients of $\mathbf{T}^p_{ij}$ fail near the walls.

B. Boundary conditions

We now examine the particle dynamics simulation results for various quantities near the walls. The purpose of this subsection is to assess how well the kinetic theory predictions for boundary conditions compare with the simulations. Somewhat simpler boundary conditions are proposed in the approximate model outlined in Sec. V.

The tangential components of the velocities of the two species are related by

$$V^2_t = \alpha V^1_t \quad \text{at } x_2 = \pm (h/2 - a). \tag{70}$$

Since there is no net flux of particles through the walls, the normal components of the velocity must satisfy

$$\phi_1 V^1_n = -\phi_2 V^2_n \quad \text{at } x_2 = \pm (h/2 - a). \tag{71}$$

The particle dynamics simulations for the case considered in the present study with $\alpha = 0.5$ gave $V^1_1 = 0.75V_0$, $V^2_1 = 0.35V_0$, $\phi_1 = 0.061$, $\phi_2 = 0.016$, $V^1_n = -0.18V_0$, and $V^2_n = 0.70V_0$ when extrapolated to $x_2 = h/2 - a$, in excellent agreement with the above conditions.

An alternative condition to the normal components satisfying Eq. (71) is requiring that the volumetric flux of species 1 toward the wall must equal the volumetric flux of species 2 away from the wall. The former is given by

$$(4\pi/3)a^3 \int_{c_2>0} c_2 f^1(\mathbf{c}) d\mathbf{c} = \phi_1 \left\{ \frac{V^1_2}{2}\left[2 - \mathrm{erfc}(V^1_2/\sqrt{2\mathbf{T}^1_{22}})\right] + \frac{\mathbf{T}^1_{22}}{\sqrt{2\pi \mathbf{T}^1_{22}}} \times \exp[-(V^1_2)^2/2\mathbf{T}^1_{22}] \right\}. \tag{72}$$

Since the assumed anisotropic Maxwellian velocity distribution of the particles is only an approximation, the volumetric fluxes are not expected to be in perfect agreement.

Substituting for the simulation results for $\mathbf{T}^1_{22}$, etc., extrapolated to $x_2 = h/2 - a$ yields $0.011\,43V_0$ for the rhs of the above equation. This may be compared with $\phi_1 V^1_2 = 0.010\,96V_0$, a difference of about 5%. On the other hand, an integral similar to the one in Eq. (72) may be evaluated for the wall-excited species. This results in $-0.011\,22V_0$ for the flux of species 2 which is essentially the same as $\phi_2 V^2_2$ obtained from the simulations.

The momentum lost (per unit time per unit area of a wall) by species 1 must equal the shear component plus the momentum flux by average motion. In other words,

$$P^1_{12} + mn_1 V^1_1 V^1_2 = m \int_{c_2>0} c_1 c_2 f^1(\mathbf{c}) d\mathbf{c} \tag{73}$$

at $x_2 = h/2 - a$. A similar condition must apply at the other wall. The integral on the rhs of the above equation can be evaluated for an assumed anisotropic Maxwellian velocity distribution to yield the following boundary condition at the wall:

$$P^1_{12} + mn_1 V^1_1 V^1_2 = mn_1\{(V^1_1 V^1_2 + \mathbf{T}^1_{12})[1 + \mathrm{erf}(V^1_2/\sqrt{2\mathbf{T}^1_{22}})]/2 + V^1_1 \sqrt{\mathbf{T}^1_{22}/2\pi}\, \exp[-(V^1_2)^2/2\mathbf{T}^1_{22}]\}. \tag{74}$$

The lhs of the above equation determined from the particle dynamics simulations and extrapolated to $x_2 = h/2 - a$ was found to equal $0.0085\rho V_0^2$. The rhs of the above equation evaluated by substituting the values of V^1_2, $\mathbf{T}^1_{22}$, etc., extrapolated from the simulation results yields $0.0087\rho V_0^2$, about 2.6% higher than the lhs. Thus, using an anisotropic Maxwellian to evaluate the momentum lost at the wall yields a reasonably accurate boundary condition. The momentum condition for species 2 may be written simply as $P^2_{12} + mn_2 V^2_1 V^2_2 = -\alpha(P^1_{12} + mn_1 V^1_1 V^1_2)$. This condition is less well satisfied by the results of particle simulations (lhs $= -0.0039$ and rhs $= -0.0042$, both nondimensionalized by ρV_0^2).

Next, the pressure component P^p_{22} is given by

$$P_{22}^1 + mn_1V_2^1V_2^1 = m\int_{c_2>0}(c_2)^2 f^1(\mathbf{c})d\mathbf{c} \quad \text{at } x_2 = h/2 - a. \tag{75}$$

An expression for the integral on the rhs of the above equation was obtained in terms of $\mathbf{T}_{22}^1$, etc., in a similar manner as in Eq. (74). This boundary condition was also found to be in good agreement with the results of numerical simulations. Similar conditions may be derived, in principle, for the components of the heat flux tensor Q_{ijk}^p. However, this will not be pursued since we do not have accurate closure relations for the heat flux tensor in the bulk.

In summary, we find that the assumed anisotropic Maxwellian form for each species can be used to prescribe accurate boundary conditions at the channel walls. In Sec. V we describe an approximate model that may be used in the absence of accurate closure relations for Q_{ijk}^p and that includes simplified boundary conditions.

V. APPROXIMATE MODEL

We have seen that most of the terms in the continuity and momentum equations for the individual species can be modeled reasonably accurately using a combination of the LV approximation (large velocity difference approximation) and either the Grad approximation or the constitutive relations suggested by Jenkins and Mancini.[26,28] The LV approximation is to be used for collisions involving species 1 and 2 for which the net velocity difference is large while the Grad or the Jenkins and Mancini approximation is to be used to account for the collisions among species of the same kind. Thus, it is unnecessary to evaluate the eightfold collision integrals described in Sec. III. The main unresolved quantity is Q_{ijk}^{pq}. In this section we shall show that a simplified model may be used to predict the profiles of volume fraction and velocity of the individual species with reasonable accuracy.

In view of the fact that we do not have satisfactory closure relations for Q_{ijk}, we shall only solve for $\mathbf{T}^1$ and $\mathbf{T}_{12}^1$. The latter is required for determining accurately the pressure component P_{12} as we saw in Sec. IV. It turns out that the closure relation for Q_{122}^1 is not crucial so that a reasonably accurate estimate of $\mathbf{T}_{12}^1$ can be obtained even with the simple closure relation for Q_{122}^1 proposed in Sec. IV. We shall also not solve for $\mathbf{T}^2$ as ϕ_2 decreases rapidly away from the wall, and near the wall the large velocity difference between the two species is more important than the temperature of species 2. We shall simply take $\mathbf{T}^2 = \mathbf{T}^1$ in the constitutive relations that require both temperatures.

We shall also assume that the velocity components parallel to the channel walls are simply related by $V_1^2 = \alpha V_1^1$. Of course, strictly speaking this is valid only at the channel walls. Since the LV approximation produces terms that are most significant near the channel walls, the above assumption will introduce negligible errors in estimating various collision-related terms. Moreover, our simulation results show that $V_1^2 = \alpha V_1^1$ is a reasonably good approximation throughout the channel width [see Fig. 16(b)].

We therefore need to solve for only seven variables as functions of x_2. These are ϕ_p, V_2^p, V_1^1, $\mathbf{T}^1$, and $\mathbf{T}_{12}^1$ $(p=1,2)$. The resulting equations are (note that $mn_p = \rho\phi_p$)

$$\frac{\partial(mn_p)}{\partial t} + \frac{\partial}{\partial x_2}(mn_pV_2^p) = \sum_{q=1}^{2}\mathbf{C}_*^{p,q}(m), \tag{76}$$

$$\frac{\partial}{\partial t}(mn_1V_1^1) + \frac{\partial}{\partial x_2}(mn_1V_1^1V_2^1 + P_{12}^1) = n_1(m_b\hat{g}_1 - \lambda V_1^1) + \chi^{1,2}(mc_1) + \mathbf{C}_*^{1,2}(mc_1), \tag{77}$$

$$\frac{\partial}{\partial t}(mn_pV_2^p) + \frac{\partial}{\partial x_2}(mn_pV_2^pV_2^p + P_{22}^p) = -n_p\lambda V_2^p + \sum_{q=1}^{2}\chi^{p,q}(mc_2) + \sum_{q=1}^{2}\mathbf{C}_*^{p,q}(mc_2), \tag{78}$$

$$\frac{\partial}{\partial t}(mn_1\mathbf{T}_{12}^1) + \frac{\partial}{\partial x_2}\left(mn_1V_2^1\mathbf{T}_{12}^1 - (4/5)k\frac{\partial\mathbf{T}_{12}^1}{\partial x_2} + \theta_2^{1,2}(mC_1C_2)\right) = -2n_1\lambda\mathbf{T}_{12}^1 - \left(P_{22}^1\frac{\partial V_1^1}{\partial x_2} + P_{12}^1\frac{\partial V_2^1}{\partial x_2}\right) + \Gamma_{12}^{1,2} + \hat{\Gamma}_{12}^{1,2}, \tag{79}$$

$$3\frac{\partial}{\partial t}(mn_1\mathbf{T}^1) + \frac{\partial}{\partial x_2}\left(3mn_1V_2^1\mathbf{T}^1 - 2k\frac{\partial\mathbf{T}^1}{\partial x_2} + \theta_2^{1,2}(mC_iC_i)\right) = -6n_1\lambda\mathbf{T}^1 - 2P_{i2}^1\frac{\partial V_i^1}{\partial x_2} + \Gamma_{ii}^{1,2} + \hat{\Gamma}_{ii}^{1,2}. \tag{80}$$

In the above equations, P_{12}^1 is evaluated using the approximation $P_{12}^1 = mn_1\mathbf{T}_{12}^1[1+(8/5)G(\phi)\phi_1] + \theta_2^{1,2}(mc_1)$. Since we shall not be explicitly solving for $\mathbf{T}_{22}^p$, it is necessary to use an approximate closure for the other pressure component, P_{22}^p. We shall use

$$P_{22}^p = mn_p\mathbf{T}^p[1+4\phi_pG(\phi)] - \frac{\phi_p}{\phi}[\kappa + (4/3)\mu_s]\frac{\partial V_2^p}{\partial x_2} + \sum_{q=1}^{2}\theta_2^{p,q}(mc_2). \tag{81}$$

The last term on the rhs of the above expression accounts for the contribution from the collision between the two species, which is evaluated using the LV approximation. (Note that according to the LV approximation, $\theta_2^{p,q}$ is nonzero only for $p \neq q$.) The first two terms on the rhs represent a slight modification of the usual dense gas theory expression. It can be shown that the implied collision part in this approximation agrees with that suggested by Jenkins and Mancini[26] for the special case $\mathbf{T}^1 = \mathbf{T}^2$ in the limit of high volume fractions (dense mixtures). Finally, κ and μ_s in the above expression and k in the equations for $\mathbf{T}^1$ and $\mathbf{T}_{12}^1$ are evaluated using the usual dense gas expressions [see Eqs. (9)–(11)]. Substituting the values of $\mathbf{T}^1$, ϕ_1, V_2^1, etc., determined from the particle dynamics simulations into the rhs of the above equation and

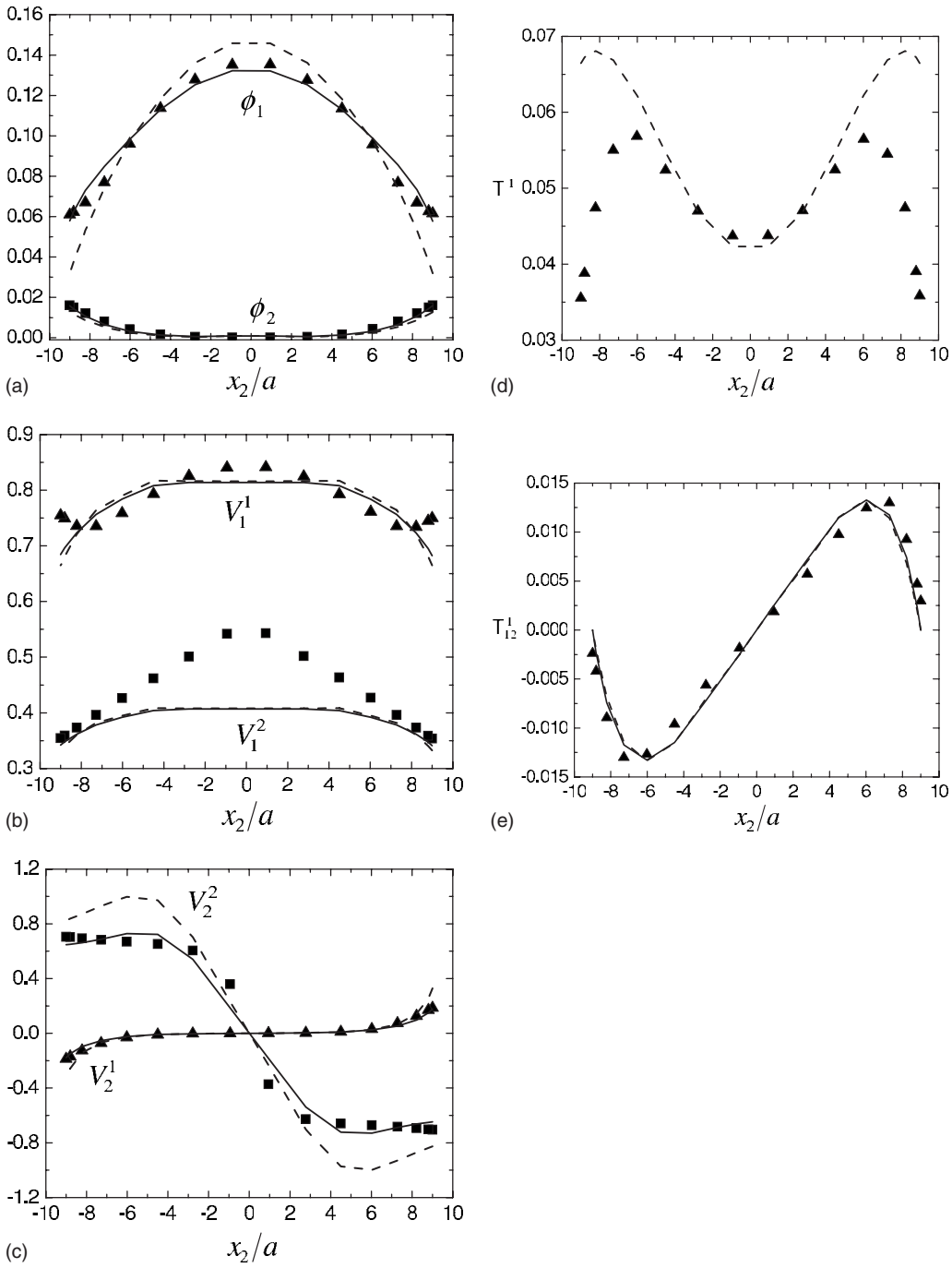

FIG. 16. A comparison between the results obtained from particle dynamics simulations and the approximate model. Symbols: particle dynamics simulations; solid line: approximate model with $\mathbf{T}^1$ taken from particle dynamics simulations; dashed line: the full model.

comparing the resulting P_{22}^1 with that determined in dynamic simulations show that the above expression provides a good estimate for values of x_2 close to the channel walls where the LV approximation makes a dominant contribution. Near the center of the channel, however, P_{22}^1 evaluated using the above expression is nearly twice that obtained from the simulations, suggesting that using the dense gas viscosity expressions results in substantial errors.

Expressions for various collision-related terms obtained using the LV approximation are summarized in Appendix B, which provides more general results for collisions involving particles of different masses or radii.

The boundary conditions are simplified as follows. Since we are expressing P_{12}^1 in terms of $\mathbf{T}_{12}^1$, the momentum equation for V_1^1 is reduced to a first-order differential equation. Therefore, no boundary conditions for this equation need to be specified at the channel walls. The symmetry condition at the channel center is sufficient. On the other hand, since we are using closure relations for P_{22}^p which are only approximate, we need to modify the boundary conditions for V_2^p at the channel walls [Eq. (75) for P_{22}^1 plus an analogous equation for P_{22}^2]. The results of particle dynamics show that V_2^1 is much smaller than V_2^2. Near the channel walls, the mean velocity component perpendicular to the wall is expected to

scale with the root-mean-squared velocity fluctuations for the normal species while the magnitude of V_2^2 is significantly larger after the collision energy contained in the velocity component parallel to the wall is partly converted into the normal component. The ratio $V_2^1/\sqrt{2\mathbf{T}_{22}^1}$ that appears in the volumetric flux condition Eq. (72) was found to be approximately constant in our particle dynamics simulations. For simulations with overall volume fractions of 0.1, 0.05, and 0.15, this ratio was found to equal, respectively, 0.92, 0.88, and 0.87. We therefore choose the following approximate boundary condition for V_2^1:

$$V_2^1 = \pm 0.9\sqrt{2\mathbf{T}_{22}^1} \quad \text{at } x_2 = \pm (h/2 - a). \tag{82}$$

We shall further approximate this condition by substituting $\mathbf{T}_{22}^1 = \mathbf{T}^1$ in the above condition as we do not explicitly solve for $\mathbf{T}_{22}^1$.

Next, the normal velocity component of species 2 is determined from energy considerations. Recall that the particles lose significant momentum in the direction parallel to the wall as a result of the collision but bounce with significantly larger normal velocity component. Requiring that the kinetic energy of the particles of species 2 leaving a wall equals γ times the energy of particles of species 1 arriving the wall yields the following condition:

$$\mathbf{L}_2 = -\gamma \mathbf{L}_1 \quad \text{at } x_2 = h/2 - a, \tag{83}$$

where $\mathbf{L}_1$ is the flux of kinetic energy of the particles of species 1 at $x_2 = h/2 - a$ and $\mathbf{L}_2$ likewise the flux of kinetic energy for species 2. It can be shown that

$$\begin{aligned}\mathbf{L}_1 = {} & (mn_1/2)V_2^1[(V_1^1)^2 + (V_2^1)^2 + \mathbf{T}_{11}^1 + 3\mathbf{T}_{22}^1 + \mathbf{T}_{33}^1] \\ & \times [1 + \mathrm{erf}(V_2^1/\sqrt{2\mathbf{T}_{22}^1})]/2 + (mn_1)/2\sqrt{\mathbf{T}_{22}^1/2\pi} \\ & \times [(V_1^1)^2 + (V_2^1)^2 + \mathbf{T}_{11}^1 + 2\mathbf{T}_{22}^1 + \mathbf{T}_{33}^1] \\ & \times \exp[-(V_2^1)^2/2\mathbf{T}_{22}^1].\end{aligned} \tag{84}$$

An expression for $\mathbf{L}_2$ can be obtained from the above equation by replacing V_1^1, V_2^1, $\mathbf{T}_{11}^1$, etc., of species 1 by, respectively, V_1^2, $-V_2^2$, $\mathbf{T}_{11}^2$, etc. Since the square of the normal velocity of species 2 is much greater than its temperature, the above condition may be simplified by neglecting $\mathbf{T}_{22}^2$ altogether, setting $\mathbf{T}_{11}^1 = \mathbf{T}_{33}^1 = \mathbf{T}_{22}^1 = \mathbf{T}^1$, and neglecting several small terms. This leads to the following approximate condition:

$$\begin{aligned}(V_2^2)^2 = {} & \frac{\gamma}{2}[(V_1^1)^2 + (V_2^1)^2 + 5\mathbf{T}^1][1 + \mathrm{erf}(V_2^1/\sqrt{2\mathbf{T}_{22}^1})] \\ & - (\alpha V_1^1)^2,\end{aligned} \tag{85}$$

where use has been made of $V_1^2 = \alpha V_1^1$. The above equation is further simplified by substituting $V_2^1 = 0.9\sqrt{2\mathbf{T}_{22}^1}$. The resulting condition gives estimates of V_2^2 in terms of V_1^1 and $\mathbf{T}_{22}^1$ that agree, when compared with those obtained from the particle dynamics simulations, within 5%, 7%, and 12% for overall volume fractions of, respectively, 0.05, 0.1, and 0.15. The condition of no net particle flux at the channel walls [see Eq. (71)] is then used to estimate ϕ_2 in terms of ϕ_1, V_2^1, and V_2^2.

Our particle dynamics simulations also showed that $\mathbf{T}_{12}^1$ is generally small at the walls. Therefore, we shall use the following simple boundary condition for solving for $\mathbf{T}_{12}^1$:

$$\mathbf{T}_{12}^1 = 0 \quad \text{at } x_2 = \pm (h/2 - a). \tag{86}$$

The condition that $\mathbf{T}_{12}^1$ at the channel walls is small can also be derived by requiring that the flux of this second moment at the channel wall must be equal to Q_{112}^1.

Finally, a boundary condition for $\mathbf{T}^1$ is obtained by equating the flux of fluctuation kinetic energy of species 1 to the conductive flux at the channel walls. After substituting $V_2^1 = 0.9\sqrt{\mathbf{T}^1}$ in the resulting expression for the flux of fluctuation energy, taking $\mathbf{T}_{11}^1 = \mathbf{T}_{22}^1 = \mathbf{T}_{33}^1 = \mathbf{T}^1$, neglecting the collisional contribution to Q_{jj2}^1, and using the limiting expression for thermal conductivity for dilute particulate systems $[k = \rho(225\sqrt{\pi}/576)\mathbf{T}^{1/2}]$, we obtain a relatively simple approximate boundary condition given by

$$\frac{\partial \mathbf{T}^1}{\partial x_2} = \pm 0.77\phi_1 \mathbf{T}^1 \quad \text{at } x_2 = \pm (a - h/2). \tag{87}$$

This condition is not well satisfied by the results obtained from particle dynamics simulations since the flux Q_{jj2}^1 obtained from the simulations deviates substantially from the assumed closure relation especially near the channel walls. Note that for dilute systems, the above condition suggests that the derivative of $\mathbf{T}^1$ near the channel walls is nearly zero whereas the particle dynamics simulations show significant gradients in $\mathbf{T}^1$ near the walls, presumably because the closure relation for the flux fails near the walls.

We now compare the profiles for various quantities obtained by solving the above set of equations with those obtained by the particle dynamics simulations. The only equation that appears to be inaccurate is the differential equation for $\mathbf{T}^1$ and the associated boundary condition. In addition, we expect some inaccuracy in our model for P_{22}^p as given by Eq. (81) although its impact should be minimal. Therefore we shall show the comparison for two cases: (i) Equation (80) for $\mathbf{T}^1$ is omitted and $\mathbf{T}^1$ required in the evaluating the particle phase viscosity in the momentum equation for V_2^p is taken from the particle dynamics simulation results. Likewise, $\mathbf{T}_{22}^1$ required in the boundary condition for V_2^1 at the channel walls is also taken from the simulations. (ii) The entire set of equations is solved including the equation for $\mathbf{T}^1$. The boundary condition for V_2^1 in this case is approximated by using $\mathbf{T}^1$ instead of $\mathbf{T}_{22}^1$. The main source of inaccuracy in case (i) is the assumed Newtonian model for the pressure components P_{22}^p. The closure relation for Q_{jj2}^1 and the boundary condition for $\mathbf{T}^1$ are the additional sources of inaccuracy in case (ii).

The numerical method for solving the averaged equations for the two species was based on a spectral collocation method.[42] Briefly, the volume fraction and velocity of the species were expressed in series of Chebyshev polynomials with the coefficients of the polynomials treated as functions of time. The governing equations were satisfied at selected values of x_2 (extrema of Chebyshev polynomials). The time derivative was discretized based on a simple two-level scheme. The nonlinear terms were approximated by a semi-

implicit scheme. Typical calculations were made using by 16 collocation points. We found that an instability occurred near the center of the channel where ϕ_2 becomes small. This instability was suppressed by setting ϕ_2/ϕ equal to 0.03 in Eq. (81) whenever ϕ_2/ϕ fell below this value.

The results for case (i) are shown in Fig. 16 by solid lines and for case (ii) by dashed lines, the particle dynamics simulations being represented by circles. We see excellent agreement for case (i) suggesting that the use of a Newtonian model for estimating the viscous stress component to P_{22}^p is adequate. In particular, the profile for $\mathbf{T}_{12}^1$, and hence the shear stress, is predicted with remarkable accuracy. The profiles for V_1^p are somewhat flatter than the ones obtained from the particle dynamics simulations and this may be attributed to the effect of inaccurate closure for P_{22}^p. Case (ii) also provides estimates that are in reasonable agreement even though we see that a significant discrepancy between the overall model and simulation results remains for $\mathbf{T}^1$, especially near the channel walls. This is largely due to the flux term which is poorly modeled by the assumed closure relation, especially near the channel walls. We found that these results are relatively insensitive to the constant (0.77) used in the mixed boundary condition (87) for $\mathbf{T}^1$.

It is interesting to note that both ϕ_2 and V_2^1 appear to decrease exponentially with distance from the channel walls. Analysis of the governing equations near the walls suggests that

$$\phi_2 = \phi_2^w \exp(-\upsilon y), \quad V_2^1 = -V_2^2(\phi_2/\phi), \tag{88}$$

where ϕ_2^w is the volume fraction at the wall, y the distance from the wall, and

$$\upsilon = -3G[\phi|\mathbf{V}^2 - \mathbf{V}^1| + (V_2^2 - V_2^1)\,\partial\phi/\partial y]/V_2^2, \tag{89}$$

where all the quantities are evaluated at the wall. These approximate relations agree very well with the particle dynamics simulations.

VI. CONCLUSIONS

We have examined in detail a model of particle-wall interactions. A simple kinetic theory was found to be inadequate for describing the profiles of particle phase volume fraction and mean velocity near the walls. The collisions render the velocity distribution near the walls significantly bimodal and anisotropic. To explore if the failure of the simple kinetic theory can be overcome if the collisional contributions to the balance equations are determined using a more accurate kinetic theory, we devised a method for treating the bimodal, anisotropic velocity fluctuations. The bimodal nature was captured by treating the particulate system as consisting of two species, and a method was devised to evaluate collision integrals when the velocity distribution of the individual species is anisotropic. We found that the kinetic theory incorporating these features does yield predictions for various quantities in mass and momentum balance equations that are in excellent agreement with the results of numerical simulations.

One of the important by-products of the study was a model which may be used as a testbed for validating the balance equations and closure relations for bidisperse systems. Previously, Kumaran *et al.*[43] examined a bidisperse macroscopically homogeneous system by Monte Carlo simulations and through a trial function for the velocity distribution. They determined collisional exchange of momentum and energy but not the transport properties required for flux calculations in flows with macroscopic gradients in particle volume fractions and velocity. In the model examined here, the relative velocity of the two species was large compared with the individual species temperatures. The closure relations derived here may be added to those suggested by Jenkins and Mancini[26,28] or Lathouwers and Bellan[33] which are applicable in the opposite limit of large species temperatures. The modifications required to account for the inelastic collisions, or unequal mass or radius, are relatively straightforward and given in Appendix B.

Our motivation for examining this model of particle-wall interactions came from the need to determine the boundary conditions for the bubble-phase continuum. It appears that the presence of walls will significantly alter the profiles of bubble-phase volume fraction and velocity. Accounting for these effects will require a more complex description of the bubble-phase equations than the ones given in the literature, e.g., by Spelt and Sangani.[10] This must be kept in mind in interpreting recent experiments, e.g., by Zenit *et al.*,[21,22] on flow of bubbly liquids in vertical and inclined channels where the root-mean-squared velocity fluctuations were small compared with the mean bubble velocity. Our analysis was restricted to a highly specialized case that did not account for the important effect of the lift force which can alter significantly the bubble volume fraction profile. Accounting for this force requires solving for the liquid phase velocity in addition to the bubble-phase equations. In view of the complexity in the resulting description, it may prove easier to combine an averaged equation description for the liquid phase with a simulation accounting for the bubble-bubble, bubble-liquid, and bubble-wall interactions.

ACKNOWLEDGMENTS

This work was supported by NASA under Grant No. 13-21407-00013-01002-001.

APPENDIX A: FORMULAS FOR EVALUATING COLLISION INTEGRALS

The following integration results are useful in the calculation of analytical integration over $\mathbf{c}'$:

$$\int E_1(\mathbf{c}',\mathbf{g})d\mathbf{c}' = \Omega^{p,q,(1)}, \tag{A1}$$

$$\int c_i' E_1(\mathbf{c}',\mathbf{g})d\mathbf{c}' = \Omega^{p,q,(1)} W_i^{p,q}, \tag{A2}$$

$$\int c_i' c_j' E_1(\mathbf{c}',\mathbf{g})d\mathbf{c}' = \Omega^{p,q,(1)}(\mathbf{T}_{ij}^m + W_i^{p,q} W_j^{p,q}), \tag{A3}$$

$$\int c_i' c_j' c_k' E_1(\mathbf{c}', \mathbf{g}) d\mathbf{c}' = \Omega^{p,q,(1)} (\mathbf{T}_{ij}^m W_k^{p,q} + \mathbf{T}_{jk}^m W_i^{p,q} + \mathbf{T}_{ik}^m W_j^{p,q} + W_i^{p,q} W_j^{p,q} W_k^{p,q}). \quad \text{(A4)}$$

In the above equations $\Omega^{p,q,(1)} = (2\pi)^{3/2} \|\mathbf{A}^{p,q}\|^{-1/2}$ and $\mathbf{T}^m = (\mathbf{A}^{p,q})^{-1}$.

APPENDIX B: FORMULAS FOR VARIOUS COLLISION-RELATED SOURCE AND FLUX TERMS USING THE LV APPROXIMATION

We give here detailed expressions for various collision-related source and flux terms in the limit when the velocity difference is large compared with the root-mean-squared fluctuation velocities of the particles. In view of their potential application to bidisperse granular flows, the expressions below are generalized to particles of unequal mass, radius, or coefficient of restitution. These expressions should be added to the expressions given by Jenkins and Mancini[26,28] to obtain approximate closure relations.

The resulting expressions from the collision of two particles labeled p and q with their masses m_p and m_q, radii a_p and a_q, inelastic collision characterized by the coefficient of restitution $e^{p,q}$ are given below with $\sigma^{p,q} = a_p + a_q$, $m_{pq} = m_p + m_q$, $M_q = m_q / m_{pq}$, $\mathbf{V}_i^{p,q} = V_i^p - V_i^q$, and $|\mathbf{V}^{p,q}| = |\mathbf{V}^p - \mathbf{V}^q|$.

- Constitutive relations for the terms in the kinetic theory of nonreacting bidisperse particulate system:

$$\chi^{p,q}(m_p c_i) = -(\sigma^{p,q})^2 G \pi (m_p m_q / m_{pq})(1 + e^{p,q}) \left\{ \frac{1}{2} n_p n_q (V_i^p - V_i^q) |\mathbf{V}^p - \mathbf{V}^q| + \frac{\sigma^{p,q}}{15} [2(V_i^p - V_i^q)(V_j^p - V_j^q) + \delta_{ij} |\mathbf{V}^p - \mathbf{V}^q|^2] \times \left(n_p \frac{\partial n_q}{\partial x_j} - n_q \frac{\partial n_p}{\partial x_j} \right) \right\}, \quad \text{(B1)}$$

$$\theta_j^{p,q}(m_p c_i) = (\sigma^{p,q})^3 \frac{\pi}{15} G (m_p m_q / m_{pq})(1 + e^{p,q}) n_p n_q [2\mathbf{V}_i^{p,q} \mathbf{V}_j^{p,q} + |\mathbf{V}^{p,q}|^2 \delta_{ij}], \quad \text{(B2)}$$

$$\chi^{p,q}(m_p c_i c_j) = (\sigma^{p,q})^2 m_p G \left\{ \frac{\pi}{2} n_p n_q M_q (1 + e^{p,q}) [|\mathbf{V}^{p,q}| (-V_i^p \mathbf{V}_j^{p,q} - V_j^p \mathbf{V}_i^{p,q}) + M_q (1 + e^{p,q})(\mathbf{V}_i^{p,q} \mathbf{V}_j^{p,q} / 2 + |\mathbf{V}^{p,q}|^2 \delta_{ij} / 6)] + \frac{2\pi}{15} \frac{\sigma^{p,q}}{2} \left(n_p \frac{\partial n_q}{\partial x_k} - n_q \frac{\partial n_p}{\partial x_k} \right) M_q (1 + e^{p,q}) \left[-V_i^p (2\mathbf{V}_j^{p,q} \mathbf{V}_k^{p,q} + |\mathbf{V}^{p,q}|^2 \delta_{jk}) - V_j^p (2\mathbf{V}_i^{p,q} \mathbf{V}_k^{p,q} + |\mathbf{V}^{p,q}|^2 \delta_{ik}) + \frac{3}{7} M_q (1 + e^{p,q}) [2\mathbf{V}_i^{p,q} \mathbf{V}_j^{p,q} \mathbf{V}_k^{p,q} + |\mathbf{V}^{p,q}|^2 (\mathbf{V}_i^{p,q} \delta_{jk} + \mathbf{V}_j^{p,q} \delta_{ik} + \mathbf{V}_k^{p,q} \delta_{ij})] \right] \right\}, \quad \text{(B3)}$$

$$\theta_k^{p,q}(m_p c_i c_j) = -\frac{(\sigma^{p,q})^3}{15} G m_p \pi n_p n_q \left\{ -V_i^p (2\mathbf{V}_j^{p,q} \mathbf{V}_k^{p,q} + |\mathbf{V}^{p,q}|^2 \delta_{jk}) - V_j^p (2\mathbf{V}_i^{p,q} \mathbf{V}_k^{p,q} + |\mathbf{V}^{p,q}|^2 \delta_{ik}) + \frac{3}{7} M_q (1 + e^{p,q}) \times [2\mathbf{V}_i^{p,q} \mathbf{V}_j^{p,q} \mathbf{V}_k^{p,q} + |\mathbf{V}^{p,q}|^2 (\mathbf{V}_i^{p,q} \delta_{jk} + \mathbf{V}_j^{p,q} \delta_{ik} + \mathbf{V}_k^{p,q} \delta_{ij})] \right\}. \quad \text{(B4)}$$

- Constitutive relations for the terms arising from the conversion of species:

$$S^{2,q}(m_2) = (\sigma^{2,q})^2 G m_2 \pi \left[n_2 n_q |\mathbf{V}^2 - \mathbf{V}^q| + \frac{\sigma^{2,q}}{2} \left(n_2 \frac{\partial n_q}{\partial x_j} - n_q \frac{\partial n_2}{\partial x_j} \right) (V_j^2 - V_j^q) \right], \quad \text{(B5)}$$

$$\hat{\theta}_j^{2,q}(m_2) = -\frac{(\sigma^{2,q})^3}{2} G m_2 \pi n_2 n_q (V_j^2 - V_j^q), \quad \text{(B6)}$$

$$S^{2,q}(m_2 c_i) = (\sigma^{2,q})^2 G m_2 \pi \left\{ V_i^2 \left[n_2 n_q |\mathbf{V}^2 - \mathbf{V}^q| + \frac{\sigma^{2,q}}{3} (V_j^2 - V_j^q) \left(n_2 \frac{\partial n_q}{\partial x_j} - n_q \frac{\partial n_2}{\partial x_j} \right) \right] - \frac{1}{2} n_2 n_q M_q (1 + e^{2,q})(V_i^2 - V_i^q) |\mathbf{V}^2 - \mathbf{V}^q| - \frac{\sigma^{2,q}}{15} M_q (1 + e^{2,q}) \left(n_2 \frac{\partial n_q}{\partial x_j} - n_q \frac{\partial n_2}{\partial x_j} \right) [2(V_i^2 - V_i^q)(V_j^2 - V_j^q) + \delta_{ij} |\mathbf{V}^2 - \mathbf{V}^q|^2] \right\}, \quad \text{(B7)}$$

$$\hat{\theta}_j^{2,q}(m_2 c_i) = -\frac{(\sigma^{2,q})^3}{2} n_2 n_q G m_2 \pi \left\{ \frac{2}{3} V_i^2 (V_j^2 - V_j^q) - \frac{2}{15} M_q (1 + e^{2,q}) [2(V_i^2 - V_i^q)(V_j^2 - V_j^q) + \delta_{ij} |\mathbf{V}^2 - \mathbf{V}^q|^2] \right\}, \quad \text{(B8)}$$

$$S^{2,q}(m_2c_ic_j) = \chi^{2,q}(m_2c_ic_j) + (\sigma^{2,q})^2 G m_2 \pi \left[n_2 n_q V_i^2 V_j^2 |\mathbf{V}^{2,q}| + \frac{\sigma^{2,q}}{3}\left(n_2 \frac{\partial n_q}{\partial x_k} - n_q \frac{\partial n_2}{\partial x_k} \right) V_i^2 V_j^2 \mathbf{V}_k^{2,q} \right], \tag{B9}$$

$$\hat{\theta}_k^{2,q}(m_2c_ic_j) = \theta_k^{2,q}(m_2c_ic_j) - \frac{(\sigma^{2,q})^3}{3} G m_2 \pi n_2 n_q V_i^2 V_j^2 \mathbf{V}_k^{2,q}. \tag{B10}$$

[1] A. Biesheuvel and L. van Wijngaarden, "Two-phase flow equations for a dilute dispersion of gas bubbles in liquid," J. Fluid Mech. **148**, 301 (1984).
[2] D. Z. Zhang and A. Prosperetti, "Averaged equations for inviscid disperse two-phase flow," J. Fluid Mech. **267**, 185 (1994).
[3] D. Z. Zhang and A. Prosperetti, "Momentum and energy equations for disperse two-phase flows and their closure for dilute suspensions," Int. J. Multiphase Flow **23**, 425 (1997).
[4] A. Esmaeeli and G. Tryggvason, "Direct numerical simulations of bubbly flows. Part 1. Low Reynolds number arrays," J. Fluid Mech. **377**, 313 (1998).
[5] A. Esmaeeli and G. Tryggvason, "Direct numerical simulations of bubbly flows. Part 2. Moderate Reynolds number arrays," J. Fluid Mech. **385**, 325 (1999).
[6] D. Drew and R. T. Lahey, "Applications of general constitutive principles to the derivation of multidimensional two-phase flow equations," Int. J. Multiphase Flow **5**, 243 (1979).
[7] S. So, H. Morikita, S. Takagi, and Y. Matsumoto, "Laser Doppler velocity measurement of turbulent bubbly channel flow," Exp. Fluids **33**, 135 (2002).
[8] A. S. Sangani and A. K. Didwania, "Dispersed-phase stress tensor of bubbly liquids at large Reynolds numbers," J. Fluid Mech. **248**, 27 (1993).
[9] S.-Y. Kang, A. S. Sangani, H.-K. Tsao, and D. L. Koch, "Rheology of dense bubble suspensions," Phys. Fluids **9**, 1540 (1997).
[10] P. D. M. Spelt and A. S. Sangani, "Properties and averaged equations for flows of bubbly liquids," Appl. Sci. Res. **58**, 337 (1997).
[11] B. U. Felderhof, "Virtual mass and drag in two-phase flow," J. Fluid Mech. **225**, 177 (1991).
[12] A. S. Sangani, D. Z. Zhang, and A. Prosperetti, "The added mass, Basset, and viscous drag coefficients in nondilute bubbly liquids undergoing small-amplitude oscillatory motion," Phys. Fluids A **3**, 2955 (1991).
[13] V. Kumaran and D. L. Koch, "The effect of hydrodynamic interactions on the average properties of a bidisperse suspension of high Reynolds number, low Weber number bubbles," Phys. Fluids A **5**, 1123 (1993).
[14] H. F. Bulthuis, A. Prosperetti, and A. S. Sangani, "Particle stress in disperse two-phase potential flow," J. Fluid Mech. **294**, 1 (1995).
[15] A. S. Sangani and A. K. Didwania, "Dynamic simulations of flows of bubbly liquids at large Reynolds numbers," J. Fluid Mech. **250**, 307 (1993).
[16] J. B. W. Kok, "Dynamics of gas bubbles moving through liquid," Ph.D. thesis, University of Twente, 1989.
[17] J. B. W. Kok, "Dynamics of a pair of gas bubbles moving through liquid. Part I. Theory," Eur. J. Mech. B/Fluids **12**, 515 (1993).
[18] J. B. W. Kok, "Dynamics of a pair of gas bubbles moving through liquid. Part II. Experiments," Eur. J. Mech. B/Fluids **12**, 541 (1993).
[19] P. C. Duineveld, "Bouncing and coalescence of two bubbles in water," Ph.D. thesis, University of Twente, 1994.
[20] R. R. Lessard and S. A. Zieminski, "Bubble coalescence and gas transfer in aqueous electrolytic solutions," Ind. Eng. Chem. Fundam. **10**, 260 (1971).
[21] R. Zenit, D. L. Koch, and A. S. Sangani, "Measurements of the average properties of a suspension of bubbles rising in a vertical channel," J. Fluid Mech. **429**, 307 (2001).
[22] R. Zenit, Y. H. Tsang, D. L. Koch, and A. S. Sangani, "Shear flow of a suspension of bubbles rising in an inclined channel," J. Fluid Mech. **515**, 261 (2004).
[23] Y. Yurkovetsky and J. F. Brady, "Statistical mechanics of bubbly liquids," Phys. Fluids **8**, 881 (1996).
[24] S. Chapman and T. G. Cowling, *The Mathematical Theory of Non-Uniform Gases*, 3rd ed. (Cambridge University Press, Cambridge, 1970).
[25] J. T. Jenkins and M. W. Richman, "Grad's 13-moment system for a dense gas of inelastic spheres," Arch. Ration. Mech. Anal. **87**, 355 (1985).
[26] J. T. Jenkins and F. Mancini, "Balance laws and constitutive relations for plane flows of a dense, binary mixture of smooth, nearly elastic, circular disks," J. Appl. Mech. **54**, 27 (1987).
[27] J. T. Jenkins and S. B. Savage, "A theory for the rapid flow of identical, smooth, nearly elastic, spherical particles," J. Fluid Mech. **130**, 187 (1983).
[28] J. T. Jenkins and F. Mancini, "Kinetic theory for binary mixtures of smooth, nearly elastic spheres," Phys. Fluids A **1**, 2050 (1989).
[29] C. K. K. Lun, S. B. Savage, D. J. Jeffrey, and N. Chepurniy, "Kinetic theories for granular flow: Inelastic particles in Couette flow and slightly inelastic particles in a general flow field," J. Fluid Mech. **140**, 223 (1984).
[30] G. Russo and P. Smereka, "Kinetic theory for bubbly flow. I. Collisionless case," SIAM J. Appl. Math. **56**, 327 (1996).
[31] G. Russo and P. Smereka, "Kinetic theory for bubbly flow. II. Fluid dynamic limit," SIAM J. Appl. Math. **56**, 358 (1996).
[32] L. Huilin, D. Gidaspow, and E. Manger, "Kinetic theory of fluidized binary granular mixtures," Phys. Rev. E **64**, 061301 (2001).
[33] D. Lathouwers and J. Bellan, "Modeling of dense gas–solid reactive mixtures applied to biomass pyrolysis in a fluidized bed," Int. J. Multiphase Flow **27**, 2155 (2001).
[34] P. Nott and J. F. Brady, "Pressure-driven flow of suspensions: Simulation and theory," J. Fluid Mech. **275**, 157 (1994).
[35] R. Verberg and D. L. Koch, "Rheology of particle suspensions with low to moderate fluid inertia and finite particle inertia," Phys. Fluids **18**, 083303 (2006).
[36] J. E. Galvin, S. R. Dahl, and C. M. Hrenya, "On the role of non-equipartition in the dynamics of rapidly flowing granular mixtures," J. Fluid Mech. **528**, 207 (2005).
[37] V. I. Kushch, A. S. Sangani, P. D. M. Spelt, and D. L. Koch, "Finite-Weber number motion of bubbles through a nearly inviscid liquid," J. Fluid Mech. **460**, 241 (2002).
[38] H. K. Tsao and D. L. Koch, "Observations of high Reynolds number bubbles interacting with a rigid wall," Phys. Fluids **9**, 44 (1997).
[39] H. Xu, M. Louge, and A. Reeves, "Solutions of the kinetic theory for bounded collisional granular flows," Continuum Mech. Thermodyn. **15**, 321 (2003).
[40] N. F. Carnahan and K. E. Starling, "Equation of state for non-attracting rigid spheres," J. Chem. Phys. **51**, 635 (1969).
[41] F. Reif, *Fundamentals of Statistical Mechanics and Thermal Physics* (McGraw-Hill, New York, 1965).
[42] R. Peyret, *Spectral Methods for Incompressible Viscous Flow, Applied Mathematical Sciences* (Springer, New York, 2002), Vol. 148.
[43] V. Kumaran, H.-K. Tsao, and D. L. Koch, "Velocity distribution function for a bidisperse, sedimenting particle-gas suspension," Int. J. Multiphase Flow **19**, 665 (1993).